SEMI ACTIVE VIBRATION CONTROL OF A SANDWICH BEAM WITH MAGNETORHEOLOGICAL ELASTOMER CORE

Major Project Report

Submitted in partial fulfillment of the requirements for the degree of

BACHELOR OF TECHNOLOGY in

MECHANICAL ENGINEERING

By,

SRIJITH KULAKATH (12ME66)

K MOHAN (12ME73)

RAHUL MADBHAVI (12ME102)

ROSHNI SAMBRANI (12ME110)

Under the guidance of

DR. S M MURIGENDRAPPA

DEPARTMENT OF MECHANICAL ENGINEERING, NITK

DEPARTMENT OF MECHANICAL ENGINEERING

NATIONAL INSTITUTE OF TECHNOLOGY KARNATAKA SURATHKAL,

MANGALORE - 575025

April, 2016

SEMI ACTIVE VIBRATION CONTROL OF A SANDWICH BEAM WITH MAGNETORHEOLOGICAL ELASTOMER CORE

Major Project Report

Submitted in partial fulfillment of the requirements for the degree of

BACHELOR OF TECHNOLOGY in

MECHANICAL ENGINEERING

By,

SRIJITH KULAKATH (12ME66)

K MOHAN (12ME73)

RAHUL MADBHAVI (12ME102)

ROSHNI SAMBRANI (12ME110)

Under the guidance of

DR. S M MURIGENDRAPPA

DEPARTMENT OF MECHANICAL ENGINEERING, NITK

DEPARTMENT OF MECHANICAL ENGINEERING

NATIONAL INSTITUTE OF TECHNOLOGY KARNATAKA SURATHKAL,

MANGALORE - 575025

April, 2016

D E C L A R A T I O N

by the B. Tech Students

We hereby *declare* that the Report of the U.G. Project Work entitled **Semi Active Vibration Control of a Sandwich Beam with Magnetorheological Elastomer Core** which is being submitted to the **National Institute of Technology Karnataka Surathkal,** in partial fulfilment of the requirements for the award of the Degree of **Bachelor of Technology** in **Mechanical Engineering** is a *bonafide report of the work carried out by us.* The material contained in this Report has not been submitted to any University or Institution for the award of any degree.

Name, Roll Number & Signature of the Students

1) SRIJITH KULAKATH (12ME66)

2) K MOHAN (12ME73)

3) RAHUL MADBHAVI (12ME102)

4) ROSHNI SAMBRANI (12ME110)

Department of Mechanical Engineering

Place: NITK, SURATHKAL

Date: May 4, 2016

C E R T I F I C A T E

This is to *certify* that the U.G. Project Work Report entitled **Semi Active Vibration Control of a Sandwich Beam with Magnetorheological Elastomer Core** submitted by,

Name, Roll Number of the Students

1) SRIJITH KULAKATH (12ME66)
2) K MOHAN (12ME73)
3) RAHUL MADBHAVI (12ME102)
4) ROSHNI SAMBRANI (12ME110)

As the record of the work carried out by them, is *accepted as the U.G. Project Work Report submission* in partial fulfillment of the requirements for the award of degree of **Bachelor of Technology** in MECHANICAL ENGINEERING

Dr. S M Murigendrappa

Project Guide

Chairman – DUGC

ACKNOWLEDGEMENT

We wish to extend our sincere gratitude to Dr. S. M. Murigendrappa, Professor, Department of Mechanical Engineering, NITK, Surathkal for providing us an opportunity to do our Major project under his guidance. We are deeply indebted for his motivation and stimulating suggestions throughout the project work.

Our heartfelt gratitude to Dr. K. V. Gangadharan, HOD, Department of Mechanical Engineering, NITK, Surathkal for his support, encouragement, and the opportunity to work in Centre for System Design (CSD) Lab and make use of the state of the art facilities available at the lab.

We sincerely thank Mr. Susheel Kumar N Sir, for his valuable guidance and sustained enthusiasm at the various stages of the project and making this a fruitful experience.

We also like to acknowledge Mr. Praveen Shenoy, Mr. Umanath R Poojari, Mr. Sai Adithya and the members of CSD LAB for their kind support, their help to make us understand concepts better and for their valuable suggestions.

ABSTRACT

The project focuses on developing control algorithm for the vibration attenuation of a sandwich beam with MRE core using semi-active vibration control methods. MREs are an important member of group of smart materials and as such have attracted increasing interest because of their modulus can be controlled by an external magnetic field.

To develop a control algorithm for any system it is essential to carry out the mathematical modelling of the system. As MRE is a visco-elastic material and is used as the core material in sandwich beam, deriving the mathematical model analytically becomes complex. Hence experimental approach for system identification was followed. To determine the mathematical model for the sandwich beam a series of free, forced, impact hammer experiments were conducted.

Based on the experimental results and the data obtained, system identification was carried out in MATLAB. System Identification tool box was used to identify the transfer functions of the system. The transfer function was identified for different magnetic fields. A comparison between the experimental results and the model predictions done using SIMULINK proved that the transfer functions can accurately predict the system behaviour under different magnetic fields.

On-Off (Bang-Bang) Controller was used to compare the response of the beam to the external excitation. In addition to this the PD controller was used to control the output of DC power supply to achieve the desired magnetic field. The use of MRE as core material for vibration attenuation of the sandwich beam was well justified.

CONTENTS

LIST OF FIGURES

LIST OF TABLES

NOMENCLATURE

APA	Amplified Piezo Actuator
CIP	Carbonyl Iron Particles
DAQ	Data Acquisition
DC	Direct Current
GUI	Graphical User Interface
LabVIEW	Laboratory Virtual Instrumentation Engineering Workbench
MR	Magnetorheological
MRE	Magnetorheological Elastomer
MRF	Magnetorheological Fluid
NI	National Instruments
T	Tesla
VI	Virtual Instrumentation

Chapter 1: Introduction

Unwanted vibrations lead to system failure, hence, its mitigation is of prime importance to the design engineer. During the recent decade, many vibration control methods have been proposed. They can be classified as:

1) Passive vibration control
2) Active vibration control
3) Semi-active vibration control

Passive vibration control systems consist of a mass, a spring and a damper. They are more stable in mitigating unwanted vibrations; however, the passive systems are only effective over a very narrow frequency range. As the excitation frequency changes, the vibration reduction effect decreases or even collapses because of mistune.

In active vibration control systems, attenuation of vibration is carried out by application of an active force by an active element. Many elements have been used as actuators ranging from piezoelectric actuators, electric motors to voice coil motors. Undoubtedly, it is a good vibration mitigation system, but still, there are disadvantages of using the active vibration system. The primary disadvantage is that they consume a lot of energy and require a large activation force (Liao et al., 2011).

Semi-active vibration control systems change their material properties and can be used in real time application without an activation force. They consume less energy in comparison to the active vibration control systems. Vibration control is achieved by varying the natural frequency of the system. This is achieved by changing the structural parameters such as: length, effective length of helical spring, effective length of cantilever beam, etc. Smart materials are used to vary stiffness and/or damping. Typically used smart materials include shape memory alloys, electro-rheological materials and magneto-rheological (Sun et al., 2015).

Nowadays smart materials such as MR are used because their rheological properties change with change in magnetic field. MR materials are usually divided into two categories: MR fluids and MR elastomers.

Although MR fluids have wide range of application , they distinct shortcomings because liquid leakage can result in environmental contamination and particle residue can degrade the use of MR devices. MR elastomers which are solid analogous of MRF may be a good solution to these shortcomings.

The present work involves the study of MRE behaviour and understanding how its field controllable modulus can be used in semi-active vibration control of the sandwich beam.

Aims and Objectives

The objectives of this project consist of fabrication, experimentation, validation and implementing of the control. The project is divided into several parts in terms of its functions of different components of the system. The specific objectives are:

1) Fabrication of the MRE.
2) Fabrication of the sandwich beam with MRE core.
3) Free vibration experiments to determine the natural frequency of the beam.
4) Modal analysis using impact hammer
5) Frequency response of the system with and without magnetic field.
6) Experiments to determine the response time of MRE core to change in magnetic field.
7) System identification using MATLAB.
8) Validation of the identified model through experiments.
9) Study and design of PID controller for the electromagnet and Bang-Bang controller for the beam control.

Chapter 2: Literature Review

2.1 Magnetorheological Materials

Magnetorheological (MR) materials are smart materials which exhibit field dependent properties. The properties of MR materials change with the application of magnetic field. This is called as MR effect. This effect was first observed by Rabinow in 1948. MR materials have developed into a family comprising of MR fluids, MR foams and MR elastomers.

The most commonly used among the MR materials are the MR fluids (MRFs). They are suspensions of magnetically polarisable particles in viscous fluids. They have been used in many applications, such as, for vibration control in automotive industry and earth quake-resistance. MRFs however, exhibit some disadvantages which limits their application. Typical problems faced when using MRFs are deposition, environmental contamination and sealing problems [Deng et al., 2008].

Solid analogy of MRF, MR Elastomers (MRE) can avoid those disadvantages associated with MRF [Dong et al., 2009]. They are composite materials composed of magnetically polarisable particles dispersed in a polymer matrix material. In the presence of magnetic field, their material properties change, hence, the particles exhibit MR effect; thus providing a field-dependent material property to the material, e.g. controllable modulus and damping. The material reclaims its original property after the magnetic field has been removed. The physical status of the material can be tuned between a soft elastomer and a semisolid, depending on the magnitude of the magnetic field applied through it.

2.1.1 Components of MRE

MR elastomers consist of three basic components: polarisable magnetic particles, an elastomeric/rubber matrix and additives (usually silicon oil). There are many materials which can be used as a matrix material. Silicone and natural rubbers are the most commonly used matrix materials. Ferromagnetic materials such as iron are used as filler particles. The components are mixed together to form a compound

with high density magnetic particles randomly dispersed or pre-arranged in a low density matrix.

The behaviour of the material is based on the interaction between the magnetic particles and the matrix in the presence of magnetic field. Due to the existence of magnetically permeable particles, the composite material exhibits a field-dependent material property subjected to the external magnetic field. A three dimensional crosslink network is formed between the adjacent magnetic particles. Such a crosslink network tends to retain its original state when external mechanical loading is applied, and the tendency is proportional to the magnetic field intensity. [Yancheng Li, *et al*, 2014].

2.1.2 MRE Types

The method of curing (Presence or absence of magnetic field) determines the structure of the MRE [Kaleta et al., 2011]. According to the way in which particles are spread, MREs are categorised as:

a) Anisotropic MRE
b) Isotropic MRE

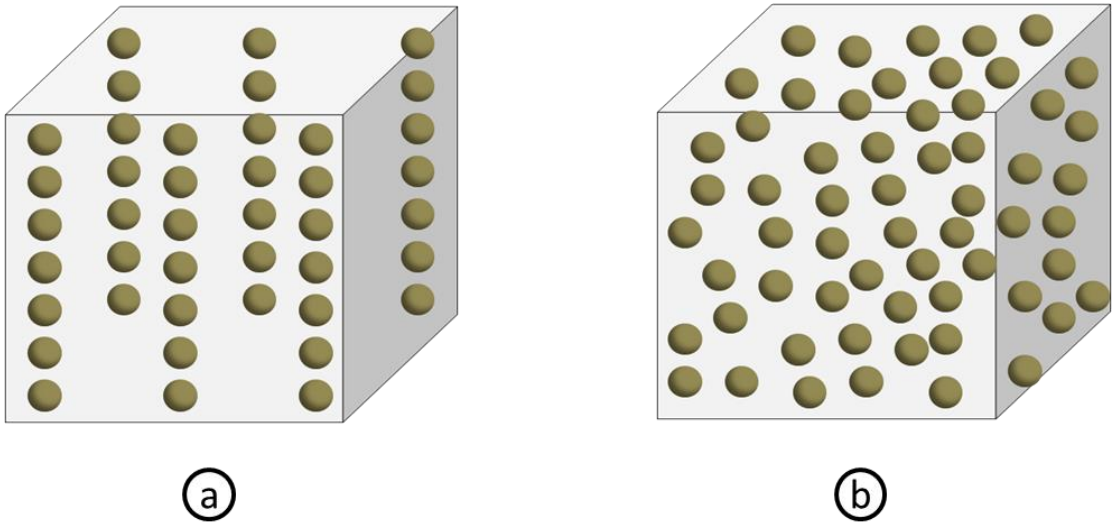

Figure 1 - MRE Types

a) Anisotropic MRE b) Isotropic MRE

Anisotropic MREs are pre-structured magnetic elastomers. They are the most investigated MREs in research. During the curing process, an external magnetic field is applied to the mixture of elastomer matrix and magnetic particles. Since, the matrix is not completely cured, the magnetic particles in the liquid can move. They align in the direction of magnetic field to form a chain-like or column structure (Figure 1). After curing, these structures get locked in the matrix.

Isotropic MR elastomers are unstructured magnetic elastomers. During the curing, no external magnetic field is applied on the mixture, and particles do not form chains or columnar structure (Figure 1) [W H. Li, et al, 2013].

2.1.3 Fabrication of MRE

The MR elastomer consists of silicone rubber as matrix material, carbonyl iron particles and additives. The process of fabrication of MRE starts by mixing all materials thoroughly. The mixture is then poured into an aluminium mould. It is then kept in a vacuum chamber to remove air bubbles. It is then left to cure for about 24 hours at room temperature with (or without) magnetic field for obtaining anisotropic (or isotropic) samples. The samples are then removed from the mould.

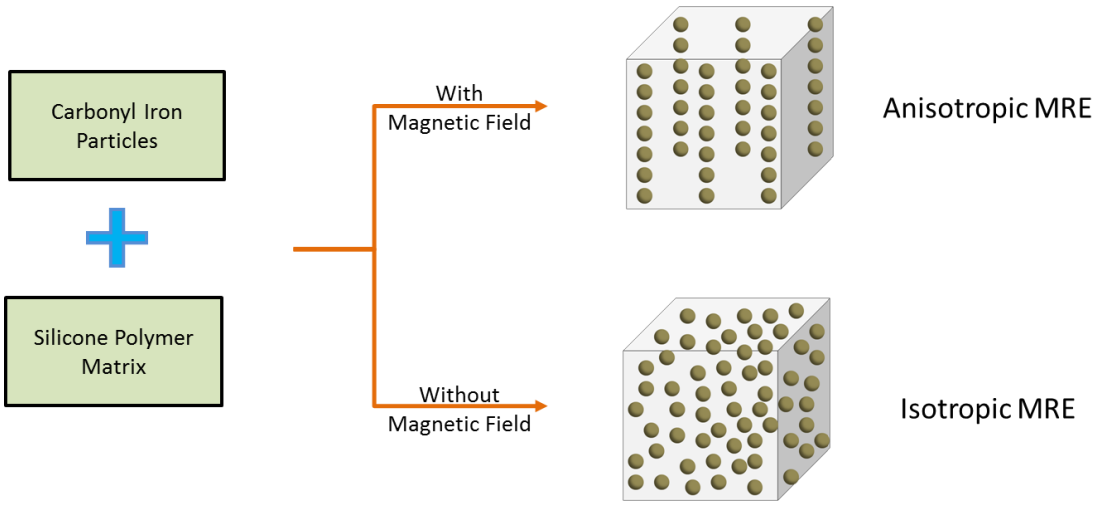

Figure 2 - Preparation of MRE

2.1.4 Modes of Operation

MREs can operate in three modes: shear mode, squeeze/elongation mode and field active mode. MREs can operate in a wide range of frequencies and have a small response time. Hence, MRE can be used as a smart material to design MRE isolators and MRE absorbers [Li et al., 2014].

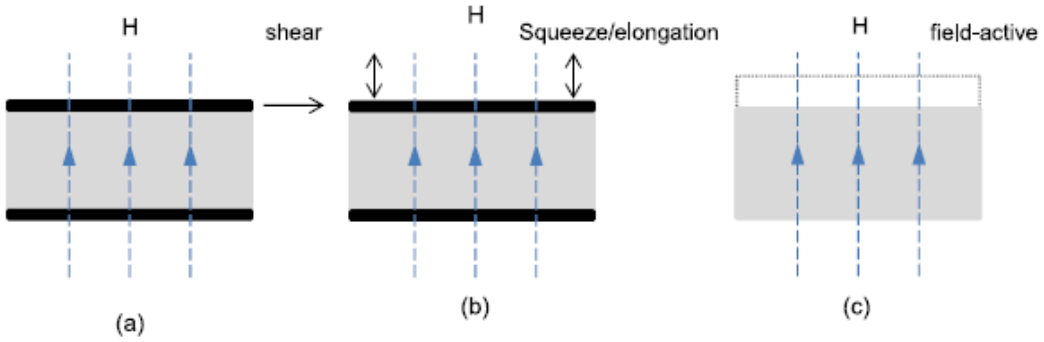

Figure 3 - Basic operation modes for MR Elastomers [Yancheng Li, et al, 2014]

a) Shear Mode b) Squeeze/Elongation Mode c) Field-active mode

2.1.4 Properties of MRE

The MR effect can be evaluated by measuring the shear strain-stress curve of sample with and without an applied magnetic field. The quasi-static shear method is generally employed to evaluate the shear modulus of MREs. Figure 4 shows the strain-stress curve of a MRE sample at seven different magnetic field intensities ranging from 0mT to 750mT with a magnetic field step increase of 125mT. The slope of the strain-stress curve is the shear modulus of the material.

The figure shows that the shear modulus of the material increases with increasing magnetic field. The shear stress shows a linear relationship with the shear strain when the strain is within 10%. This means the MRE have linear viscoelastic properties when the strain is below 10%. This finding is totally different from MR fluids in which linear viscoelastic region is only up to 0.1% strain.

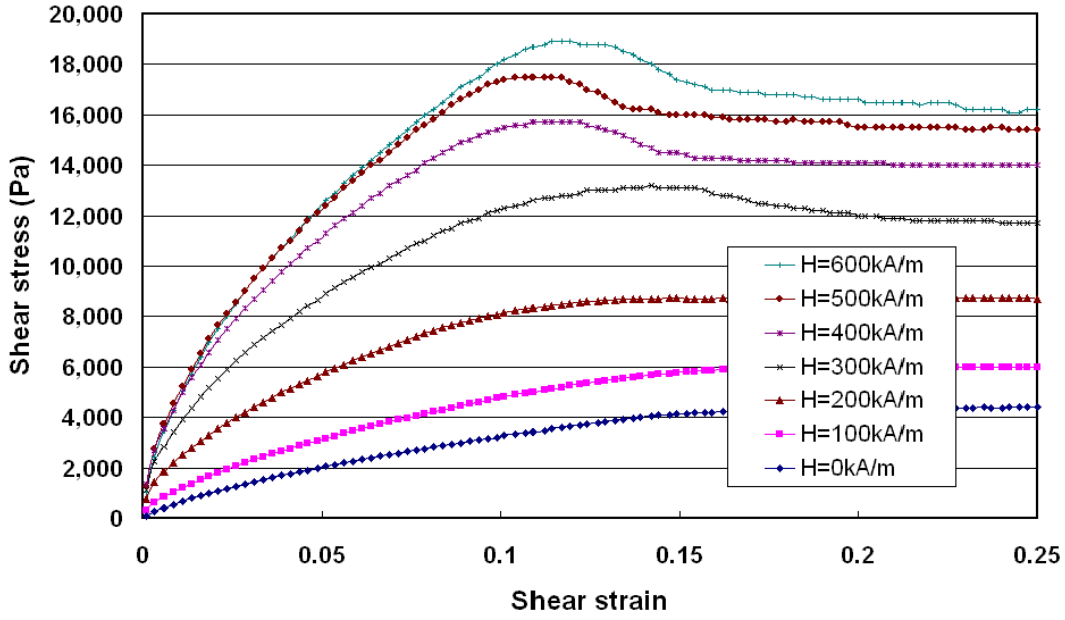

Figure 4 - Shear stress-strain curves of MRE Sample [W. H Li, 2013]

This also demonstrates that MREs generally operate in the pre-yield region while MRF operates in the post-yield region. When the strain is above 10%, the modulus reaches a maximum value and then steadily decreases, which implies that MRE enters into a nonlinear viscoelastic regime.

In the three-layered MRE sandwich beam configuration, the MRE materials experience shear stress and shear strain that is confined in the pre-yield regime. The stress-strain relationship based on linear viscoelastic theory is given by the following equation:

$$\tau = G^*\gamma$$

In the above equation, τ is shear stress, γ is shear strain, and G^* is the complex shear modulus represented in the form

$$G^* = G' + G" i$$

Where, *G'* is the storage modulus, and *G''* is the loss modulus. The storage modulus is proportional to the average energy stored during a cycle of deformation per unit volume of the MRE material. The loss modulus is proportional to the energy dissipated per unit volume of the MRE material over a cycle.

Experiments were conducted by Guoliang Hu, et al (2011) to determine the relationship between the storage modulus, the loss modulus and the applied magnetic field.

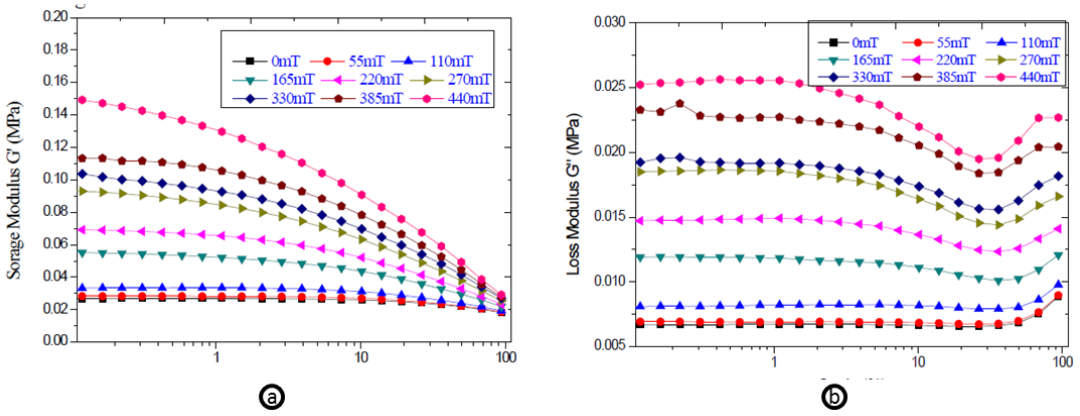

Figure 5 - Storage modulus and Loss modulus of MRE [Guoliang Hu, et al 2011]

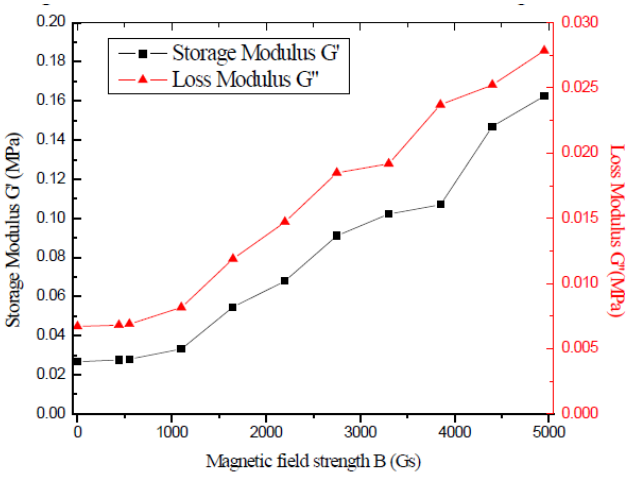

Figure 6 - Storage and Loss Moduli for different magnetic fields

[Gyoliang Hu, et al 2011]

Figure 5a shows the relationships between the storage modulus of MRE and the strain under different magnetic field, and Figure 5b shows the relationships

between the loss modulus of MRE and the strain under different magnetic field [Guoliang Hu, et al 2011].

Figure 6 shows the storage modulus and the loss modulus as a function of the magnetic field when the shear strain is below 0.01%. From the figure, it is noted that the storage modulus and the loss modulus increased as the magnetic field strength increased, and both of them increased dramatically when the magnetic field strength exceeds 100mT.

2.1.5 Stiffness of MRE

For a shear mode device with a rectangular cross section having thickness h, Shear modulus G, cross section area A and n MR elastomer layers the stiffness can be expressed as

$$K_s = \frac{GA}{nh}$$

For the squeeze mode MR elastomer devices having compression modulus E, the compressive stiffness of the device can be expressed as:

$$K_c = \frac{EA}{nh}$$

2.1.6 Natural Frequency of Sandwich Beam with MRE Core

Experiments were conducted by Guoliang Hu, et al (2011) on a sandwich beam with MRE core to determine the effect of non-homogenous magnetic field intensity on the natural frequency. During the experiments, the magnetic field intensity was changed. The magnetic field was applied on a specific region. The first natural frequency of MRE sandwich beam under different magnetic field intensity is shown on Figure 7. It is also noted that the first natural frequency of the MRE sandwich beam decreased as the magnetic field increased.

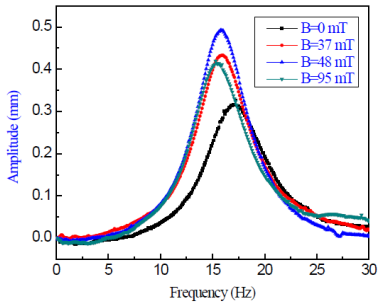

Figure 7 - Vibration response under different magnetic field intensity

[Guoliang Hu, et al, 2011]

2.1.7 Summary

Author	Parameters Varied	Parameter Values	Remarks
Li et al (2008)	Type of MRE	Anisotropic MRE	Shear and Storage Modull increase with Magnetic field
	Loading	Shear mode	
	Strain Amplitude	0.01% to 100%.	
Shen et al (2004)	Matrix	Polyurethane and natural rubber	Shear modulus of polyurethane is higher compared to natural rubber.
Li et al (2010)	Type of MRE	Anisotropic and isotropic	Anisotropic MRE exhibits higher MR effect.
	Loading	Compressive and shear loading	
Johnson et al (2012)	Thickness		storage modulus increases without magnetic field, no change in storage modulus with magnetic field.
Chen et al(2007)	Magnetic field		Shear storage modulus increased
	Percentage of CIP	80% carbonyl iron particles by weight.	
Jung et al (2009)	Percentage of CIP	30% content iron particle by volume.	Shear storage modulus and loss factor increased.
	Loading	Pre-compression-shear type combined loading.	
Lokander et al (2003)	Particle Shape	Irregular iron particles	Increase in range of the shear modulus of MRE

Table 1 - MRE Literature Review Summary

2.2 Conclusion

Magnetorheological elastomers can be used as smart materials in the implementation of semi-active vibration control. There are many parameters that influence the behaviour of MR elastomer smart devices, these include matrix material, size and shape of the iron particles, operational modes, configuration of magnetic circuit, supplied current (pulse) and control strategies. The stiffness and damping of MREs can be varied based on the magnitude of the applied magnetic field, which are the suitable properties for semi-active vibration control.

Chapter 3: Beam Fabrication

3.1 Aluminum Mould

Dimensions of the cavity:

Length (l) = 260mm (Center-Center distance, Ends rounded)

Breadth (b) = 19mm

Depth (d) = 3mm

Volume of Cavity = $lbd + \frac{\pi b^2 d}{4} = (260 \times 19 \times 3) + \frac{\pi(19)^2(3)}{4}$ = 15.7 cc

The mould cavity dimensions are shown in the Figure 8.

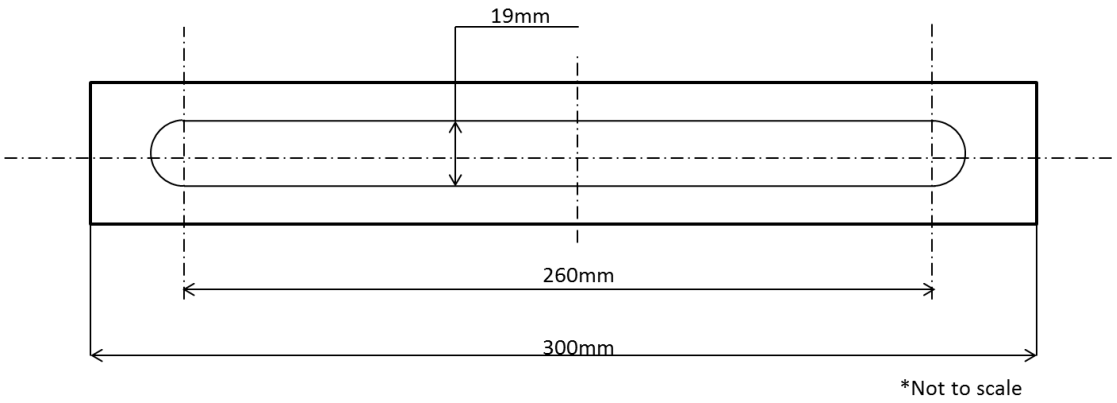

Figure 8 - Mould Dimensions Diagram

3.2 MRE Components Calculations

23.7% by volume of Iron particles (particle size: 3.15 µm) was chosen to make the MRE.

Relative Density of CIP = 7.80

Relative Density of silicone polymer matrix = 1.15

Volume of MRE Cavity = 15.7 cc.

The actual volume of MRE that was mixed was 24cc. This was due to the fact that some of the MRE sticks to the container in which it is being mixed. The weights shown below are for 24cc of MRE. The weight composition of MRE components is tabulated in Table 2 - Weight Compositions of MRE ComponentsTable 2.

Component	Weight (grams)
Carbonyl Iron particles	44.366
Silicon polymer matrix	21.059

Table 2 - Weight Compositions of MRE Components

3.3 Preparation of MRE

The basic constituents of MRE are a polymer matrix and carbonyl iron particles. The iron particles and the silicon polymer were first weighed separately in the order to get 23.7% by volume composition of the MRE. The components were then mixed and stirred in a container uniformly until no cluster of iron particles are found in the mixture. At this point the curing agent was added to the mixture and stirred again till it is distributed evenly in the mixture. The container was placed in the desiccator to remove air bubbles. The mixture was then poured in the mould. Pressure was applied on the MRE in the mould and it was allowed to cure for 24 hours.

3.4 Fabrication of Aluminum Frame of the Beam

The sandwich beam consists of MRE sandwiched between two thin strips of aluminum. Thin aluminium plates were chosen for elastic surface plates due to their low damping properties and relatively high stiffness compared to that of the MRE. Additionally, its relatively magnetic permeability is equal to one, which means that it does not affect the distribution and strength of the magnetic field. The beam's effective length is 252mm having 19mm width and is 1.5 mm thick.

3.5 Fabrication of Sandwich Beam

The structural profile of the MRE sandwich beam is shown in Figure 9. It is made of three layers: the top and bottom layers are Aluminium and the core is MRE. The MRE that was prepared was taken out of the mould and sandwiched between two

aluminium plates using adhesive. The dimensions of the aluminum frame are shown in the Figure 9.

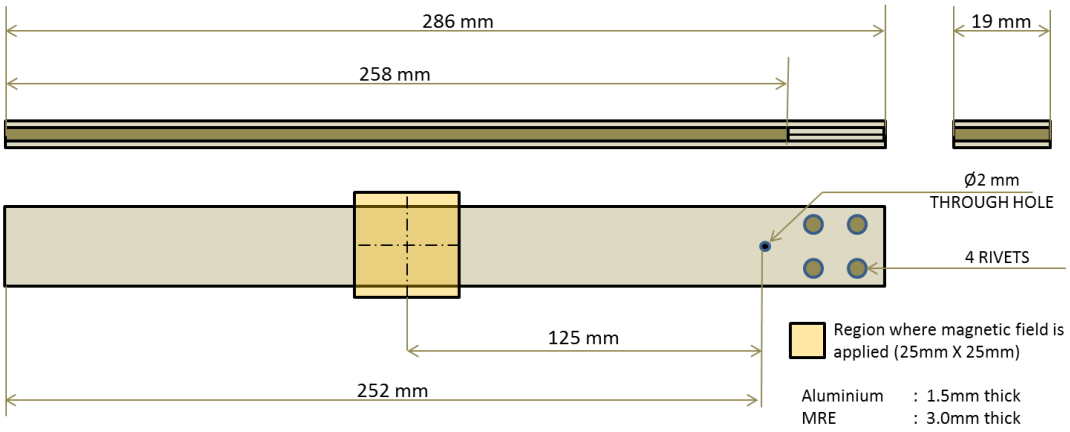

Figure 9 - Beam Dimensions

Figure 10 - MRE Sandwich Beam

Chapter 4: Experimental Setup

4.1 Hardware

Table 3 lists all the equipment used along with the model numbers and function.

Sl. No	Equipment	Model No.	Function
1	Accelerometer	KISTLER-2081	Used to measure acceleration
2	CEDRAT APA	APA120S	Piezo Stack used to excite the beam to required signals
3	Function generator	Agilent 33220A 20 MHz	Generates the required input signals
4	Programmable DC power supply	XG 850 watt	Used to control the current supply to the electromagnet through LABVIEW program
5	Power Amplifier	CEDRAT Power Amplifier	Amplifies the signals generated by the function Generator
6	Electromagnet		Used to produce Magnetic field
7	DAQ	NI-DAQ 9234	It is the input DAQ used to acquire the signals from the accelerometer
		NI-DAQ 9215	Used to determine the current flowing through the electromagnet circuit
		NI-DAQ 9264	Output DAQ used to send signals to the DC power supply.

Table 3 - Hardware used

4.2 Fabricating fixture to attach piezoelectric actuator to the beam

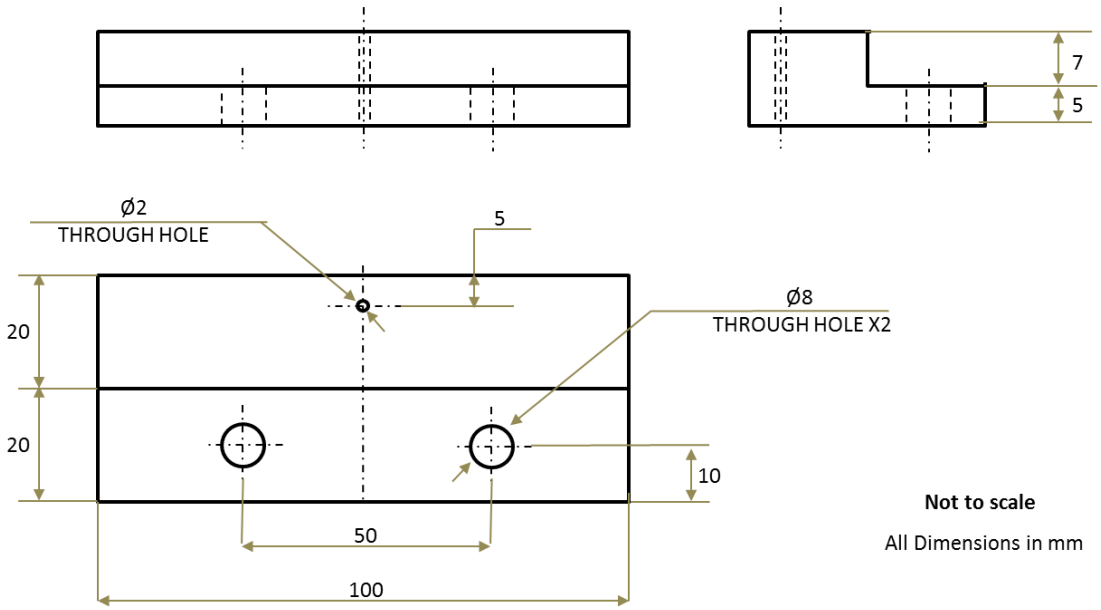

Figure 11 - Fixture dimensions

A fixture was needed to mount the piezo actuator on the beam. The dimensions of the fixture are shown in Figure 11. The mild steel block was first cut from a blank. It was then shaped in a shaper. Finally, through holes were drilled for fixing it on the base. Another through hole was drilled to allow for the piezo actuator to be fixed to it. Figure 12 shows the different machining operations and the final fixture.

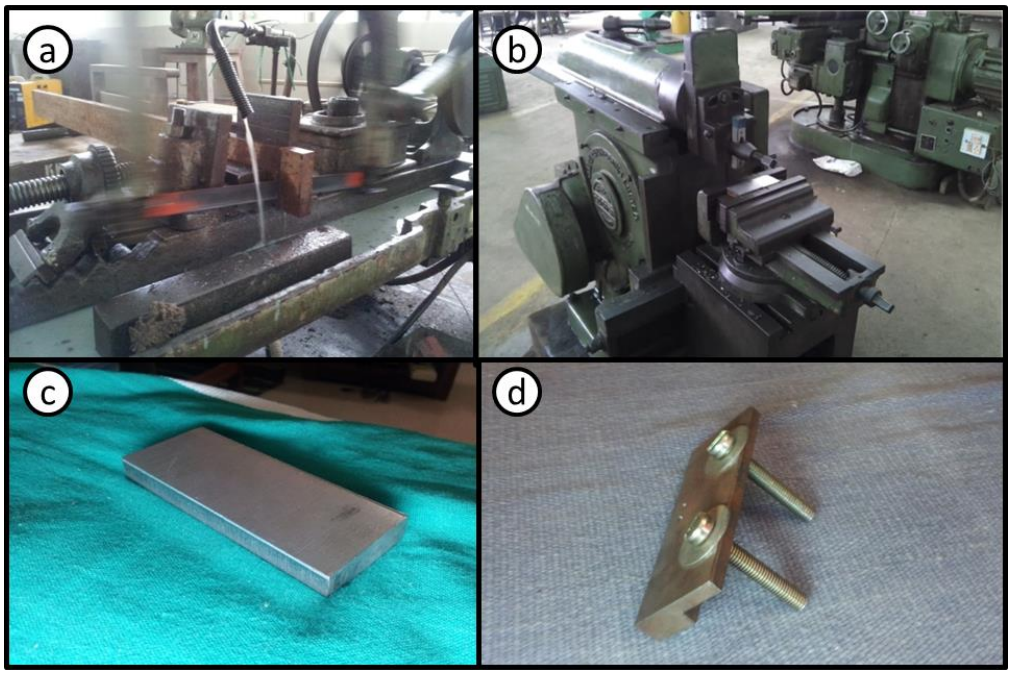

Figure 12 - Fixture fabrication

a) Blank Cutting b) Shaping c) Shaped Work piece d) Completed Fixture

4.3 Electromagnet Assembly

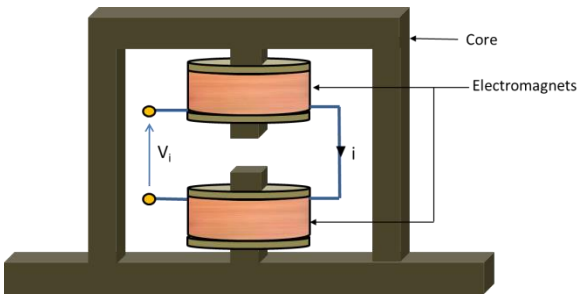

Figure 13 - Electromagnet

4.4 Mounting the accelerometer on the beam

The accelerometer was mounted on the free end of the MRE sandwich beam. Figure 14 shows the accelerometer mounted on the beam.

Figure 14 - Accelerometer mounted on the beam

4.5 Configuring hardware and Wiring

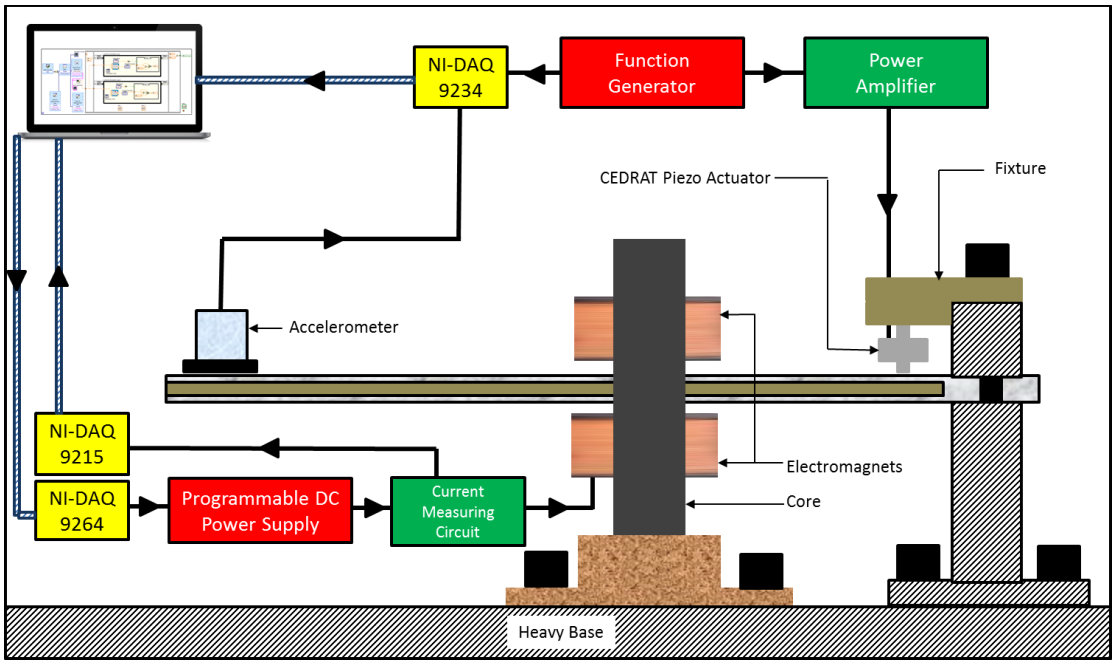

Figure 15 - Hardware setup

Chapter 5: Experiments and Simulation

5.1 Free Vibration Response

5.1.1 Procedure

The beam was given an initial displacement. The vibration data of the beam was acquired by the accelerometer connected to the computer using the NI-DAQ 9234. After obtaining the natural frequency of the beam without applying magnetic field, trials were conducted with magnetic field. The electromagnets were used to apply magnetic fields on a small region of the sandwich beam. The natural frequency of the beam was determined for different magnetic flux densities in increasing order from 50mT to 285mT (50mT, 100mT, 150mT, 200mT, 250mT, 285mT). The maximum current which could safely be given to the coils without overheating them was 4.5A. This magnitude of current resulted in the electromagnet-core setup producing 285mT.

5.1.2 LabVIEW VI

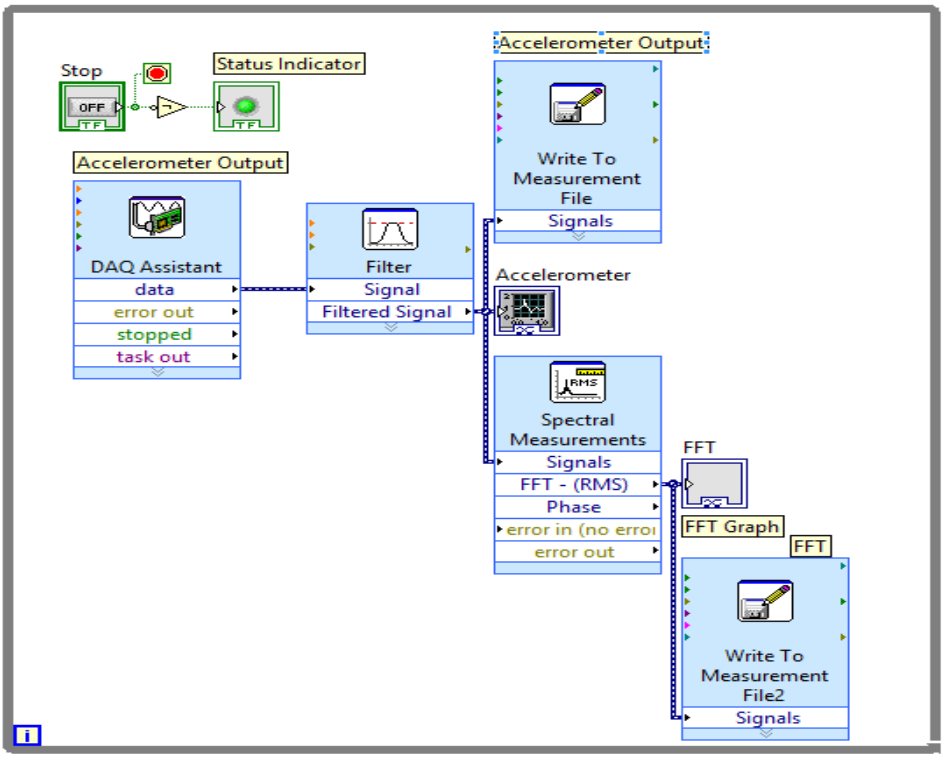

Figure 16 - Free Vibration Test LabVIEW VI

The LabVIEW VI processes the accelerometer data. The time domain vibration data is processed to get the frequency domain data. Natural frequency and amplitude of the vibration are presented in the output of the analysis results, also the time and frequency domain data are written to measurement files.

5.2 Impact Hammer Test

5.2.1 Procedure

Impact Hammer test was conducted to determine the higher natural frequencies of the MRE sandwich beam. The impact hammer was struck near the fixed support. The accelerometer was positioned at the free end of the beam. The accelerometer and impact hammer were connected to the NI-DAQ 9234.

5.2.2 LabVIEW VI

The VI used was from the Sound and Vibration Measurement Toolbox of LabVIEW. Its front panel images are as shown below.

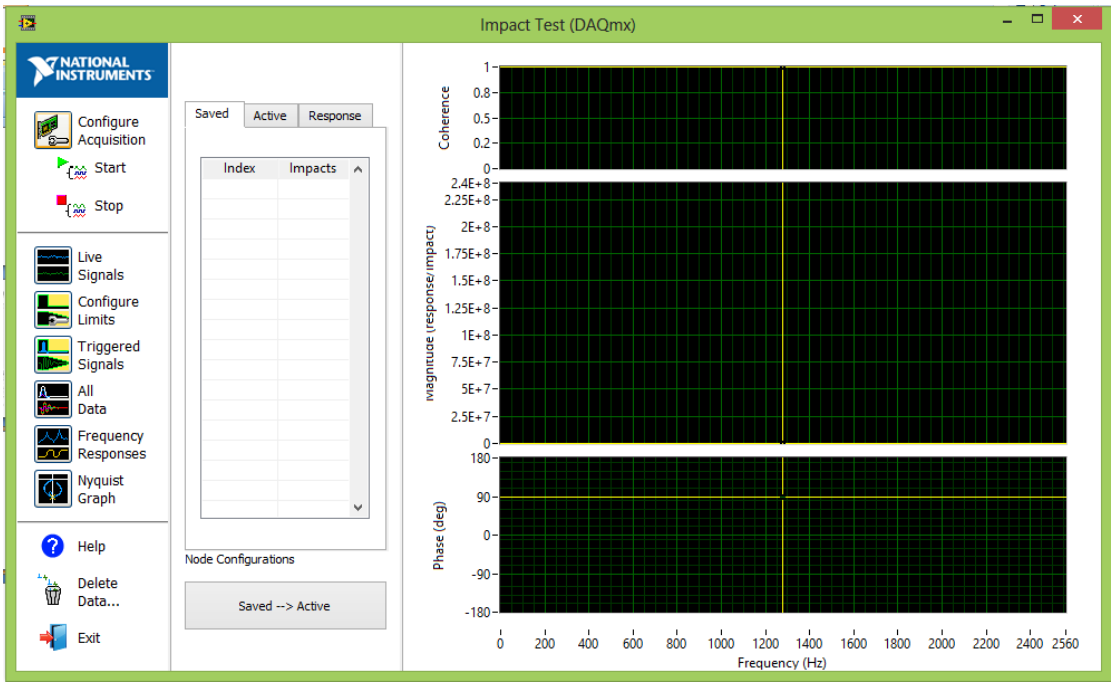

Figure 17 - LabVIEW VI for Impact Hammer Test (Front Panel)

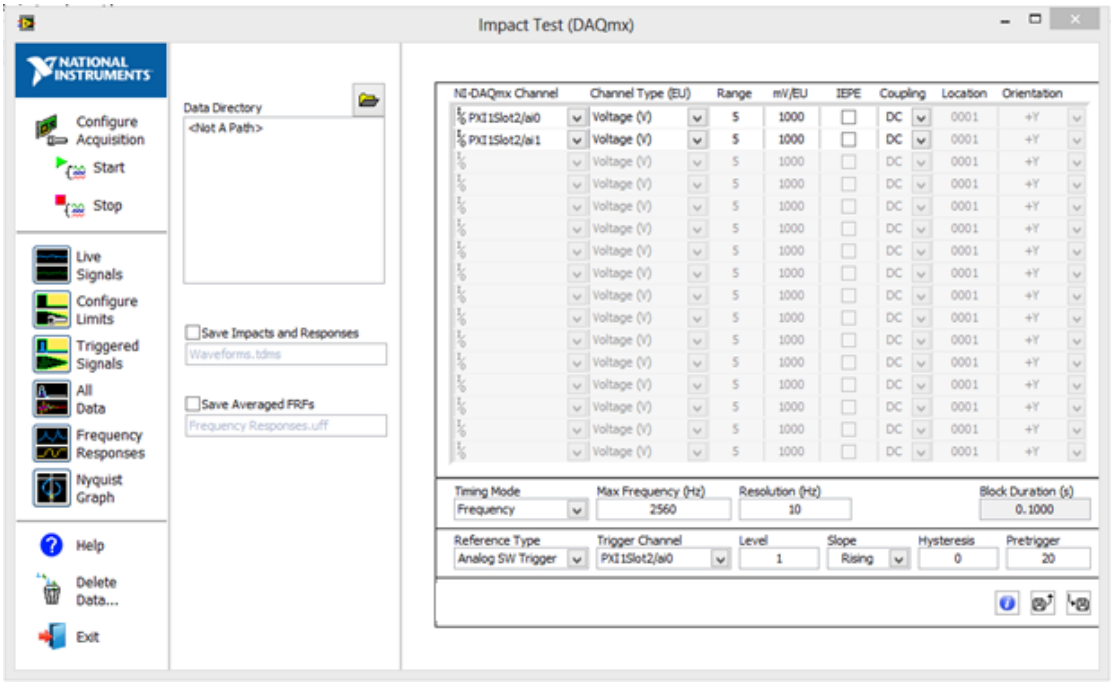

Figure 18 - LabVIEW VI for Impact Hammer Test (Configuration Panel)

5.3 Forced Vibration Response

5.3.1 Procedure

The forced vibration response is carried out to obtain time domain and frequency domain response for system identification. System identification is done to obtain transfer function of the system. The plant transfer function is required to develop control algorithm for semi-active vibration control.

Sine sweep is generated using a Function Generator. This sine sweep is an input to the CEDRAT Piezo actuator via a power amplifier. The sine sweep is given in the range of frequencies 10-25 Hz. The vibration data of the beam is acquired by the accelerometer which is connected to the computer through the NI-DAQ 9234. After conducting experiments without magnetic field, trials were conducted to obtain response of the beam under different magnetic flux density conditions (50mT, 100mT, 150mT, 200mT, 250mT and 285mT).

5.3.2 LabVIEW VI

The LabVIEW programming in the computer processes the input signal. Then, the vibration response in frequency domain, natural frequencies and amplitudes of the vibration are presented in the output of the analysis results.

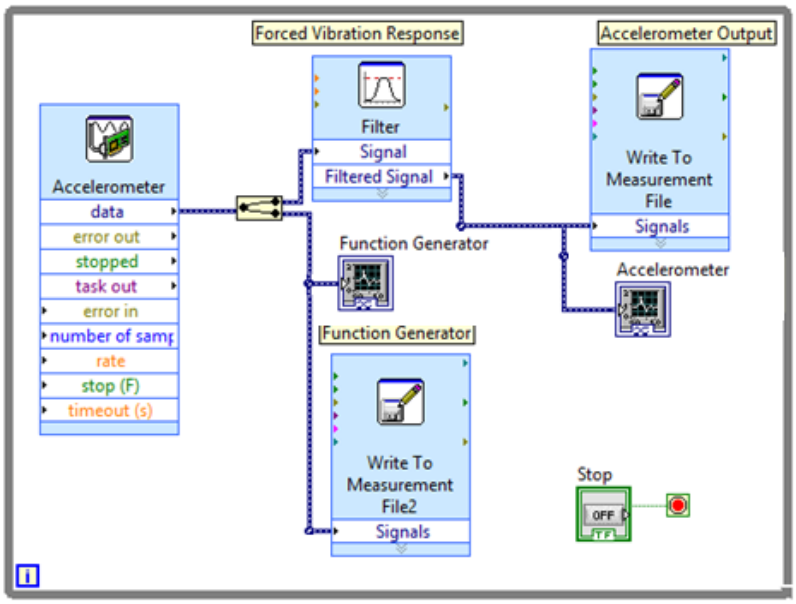

Figure 19 - LabVIEW Code to acquire Forced Vibration Data

5.4 Response Time of MRE Material to change in magnetic field

5.4.1 Procedure

A constant frequency signal is applied to the CEDRAT via power amplifier i.e. the beam is excited at a constant frequency. A step voltage input is provided to the electromagnetic coils. Thus, the beam now undergoes a transient state and finally vibrates at new amplitude. The time taken by the beam to reach the steady state field is determined from the time domain plot of accelerometer data. This gives the response time of beam.

5.4.2 LabVIEW VI

The LabVIEW VI used is the same as the VI used for forced vibration response test (Refer Figure 19)

5.5 Determining the Resistance and Inductance of the Electromagnet

5.5.1 Experimental Setup

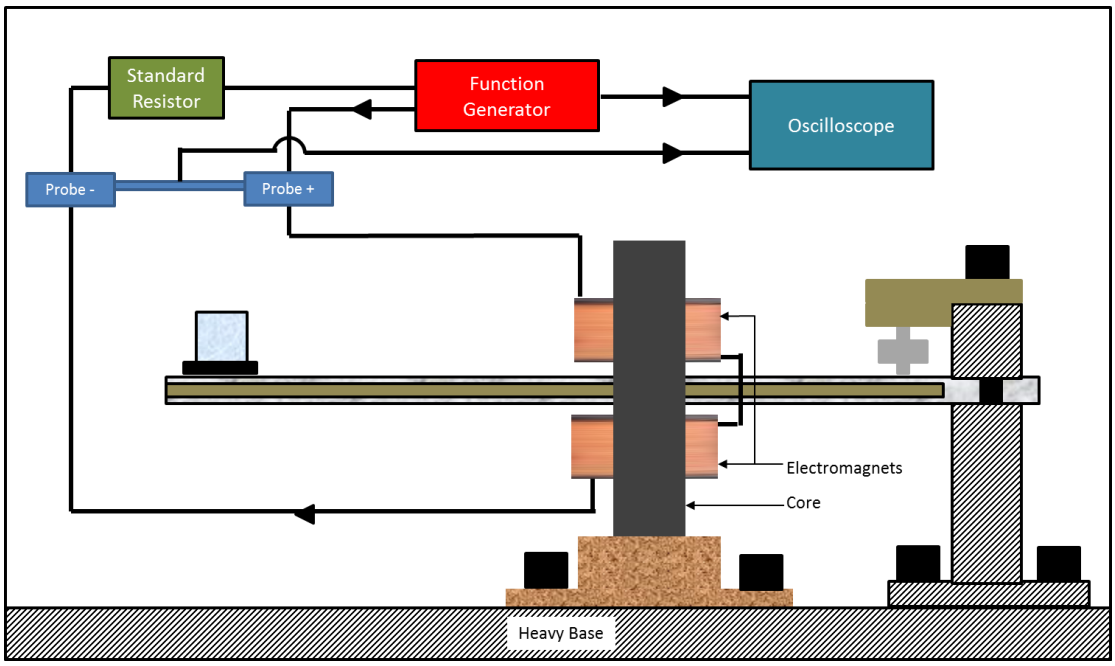

Figure 20 - Experimental Setup for finding Inductance of Electromagnet

5.5.2 Procedure

A step voltage was applied to the electromagnet, the steady state current through the coils and the voltage across them was measured. The resistance of the coil was determined by taking the ratio of the voltage across the coil to the current flowing through it. This value was verified by disconnecting the electromagnet from the circuit and measuring its resistance using a digital multimeter.

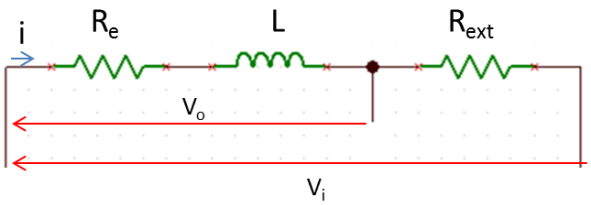

Figure 21 - Circuit Diagram of Inductance Measuring Circuit

The method used to find the inductance of the electromagnet is called as the half impedance method. The electromagnet was connected in series to a standard resistor. The end terminals of the series circuit were connected to the output of the

function generator. This output was also connected to the oscilloscope by using a BNC splitter. Oscilloscope probes are connected across the electromagnet. The function generator was configured to give sine wave outputs. The corresponding output across the electromagnet was read using the oscilloscope. The frequency at which the amplitude of the voltage output across the electromagnet is half the amplitude of the supplied voltage is determined. This is then used to calculate the inductance of the coil by using the equation:

$$L = \frac{R}{2\pi f}$$

This value was then verified by mathematically calculating the output voltage amplitude for different frequencies and comparing the results from experiments.

Here, we have the following notations being used:

Z = Total impedance of the circuit.

R_t = Total resistance in the series circuit.

R_e = Resistance of the electromagnet.

R_{ext} = Resistance of the external resistor.

L = Inductance of the coils.

ω = Circular frequency of the excitation source.

V_i = Input voltage amplitude.

V_o = Output voltage amplitude.

The total impedance across the circuit is given by:

$$Z = R_t + i(\omega L)$$

Where,

$$R_t = R_e + R_{ext}$$

Hence, the output voltage across the electromagnet is given by:

$$V_o = \frac{R_e + i(\omega L)}{R_t + i(\omega L)} \times V_i$$

Since, the inductance was determined, different values of input frequencies were used as inputs. The output was calculated using the above expression and should be verified by providing different frequency inputs and verifying the output observed with the calculated output.

5.6 System Identification

To start a new session in the System Identification app, click on the System Identification icon in the Apps tab. This opens the system identification app.

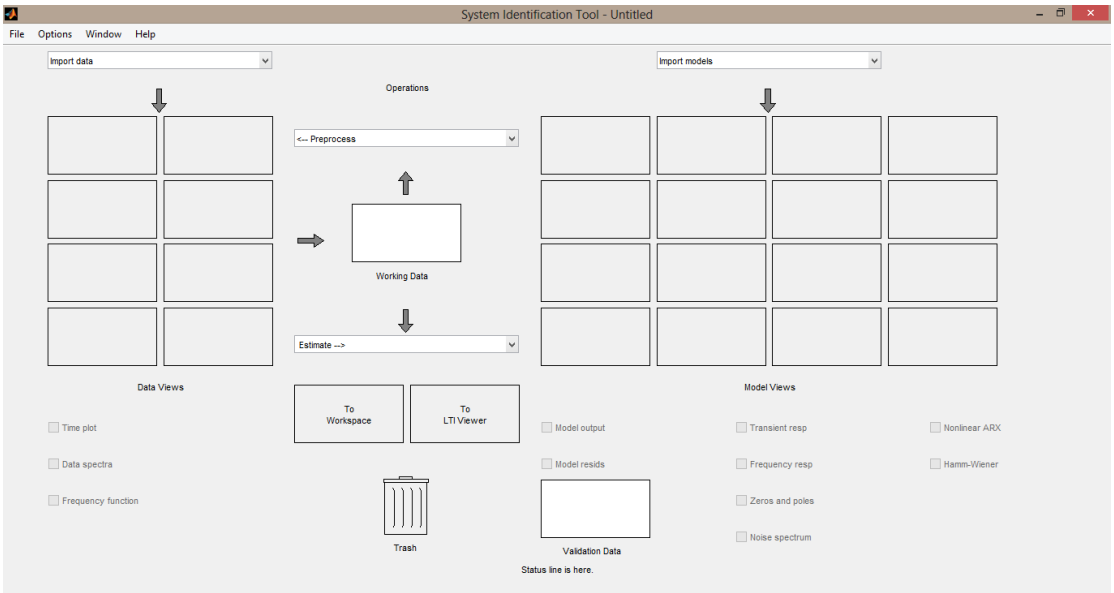

Figure 22 - MATLAB System Identification Toolbox

5.6.1 System Identification App Window

The following figure describes the different areas in the System Identification app. The layout of the window organizes tasks and information from left to right. This organization follows a typical workflow, where one starts from the top-left corner by importing data into the System Identification app using the **Import data** menu and

end in the bottom-right corner by plotting the characteristics of your estimated model on model plots.

The **Data Board** area, located below the **Import data** menu in the System Identification app, contains rectangular icons that represent the data that was imported into the app. The **Model Board**, located to the right of the **Preprocess** menu in the System Identification app, contains rectangular icons that represent the models estimated or imported into the app. Model icons can be dragged and dropped in the Model Board into open dialog boxes.

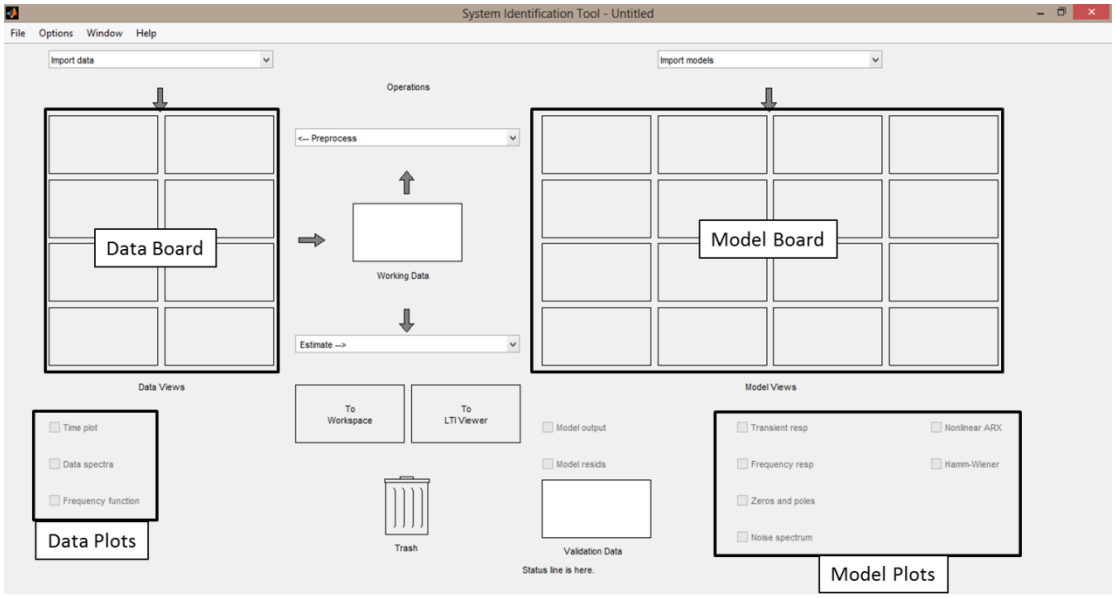

Figure 23 - MATLAB System Identification Toolbox Layout

The primary purpose why we used the system identification was to determine the system transfer function.

5.6.2 Transfer Function Models

Transfer function models describe the relationship between the outputs and inputs of a system using a ratio of polynomials. The model order is equal to the order of the denominator polynomial. The roots of the denominator polynomial are referred to as the model **poles**. The roots of the numerator polynomial are referred to as the model **zeros**.

We have estimated the transfer function models using the time domain vibration data by giving sine sweep inputs to the beam.

5.6.3 Procedure

1) Import time domain data into the System Identification app.

2) In the System Identification app, select **Estimate** > **Transfer Function Models.** The Transfer Functions dialog box opens.

3) In the **Number of poles** and **Number of zeros** fields, specify the number of poles and zeros of the transfer function as non-negative integers.

4) Select **Continuous-time** or **Discrete-time** to specify whether the model is a continuous or discrete-time transfer function.

5) Click **Estimate** to estimate the model. A new model gets added to the System Identification app.

Note: This process is an iterative process. If the system order is known, the procedure is straight forward. Since, just by giving the correct number of poles and zeros will result in getting the transfer function. However, in our case, the number of poles and zeros of the plant were not known, it required an iterative process where different combinations of poles and zeros models had to be used. We used ten trials of data for each magnetic flux density magnitudes to validate the models.

5.7 SIMULINK Simulation

5.7.1 Procedure

The models obtained are used to simulate the controller in SIMULINK. This allows for safe tuning of the system without causing damage to it. The obtained models are given experiment input data and the outputs are compared with the actual experiment outputs to check the accuracy of the models. The control algorithm is then tuned to get the gains.

5.7.2 Simulink Block Diagram

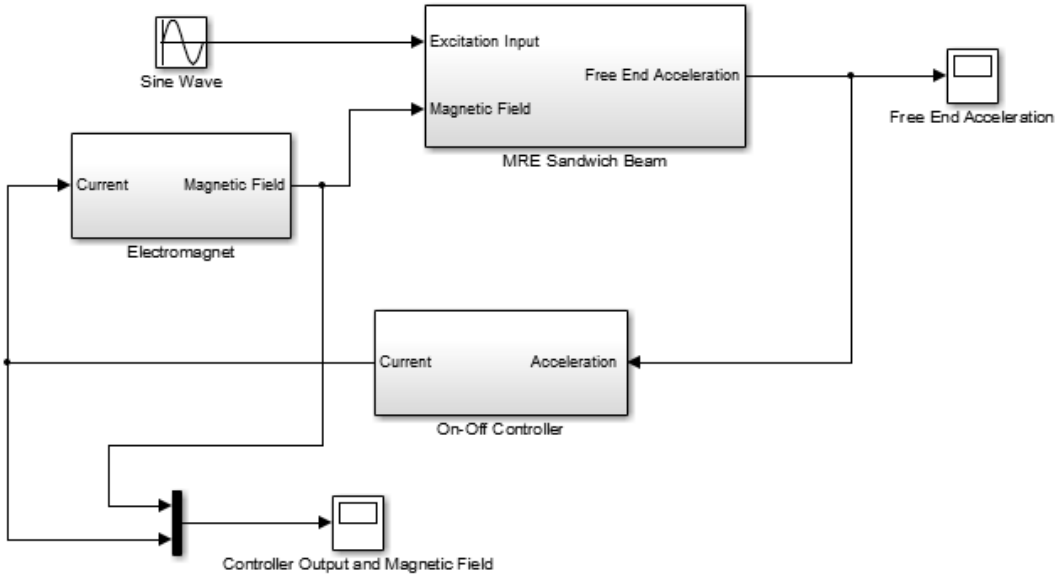

Figure 24 - MRE Sandwich Beam with Electromagnet and On-Off Controller

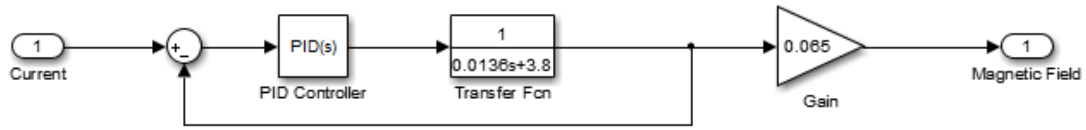

Figure 25 - Electromagnet Model with PID

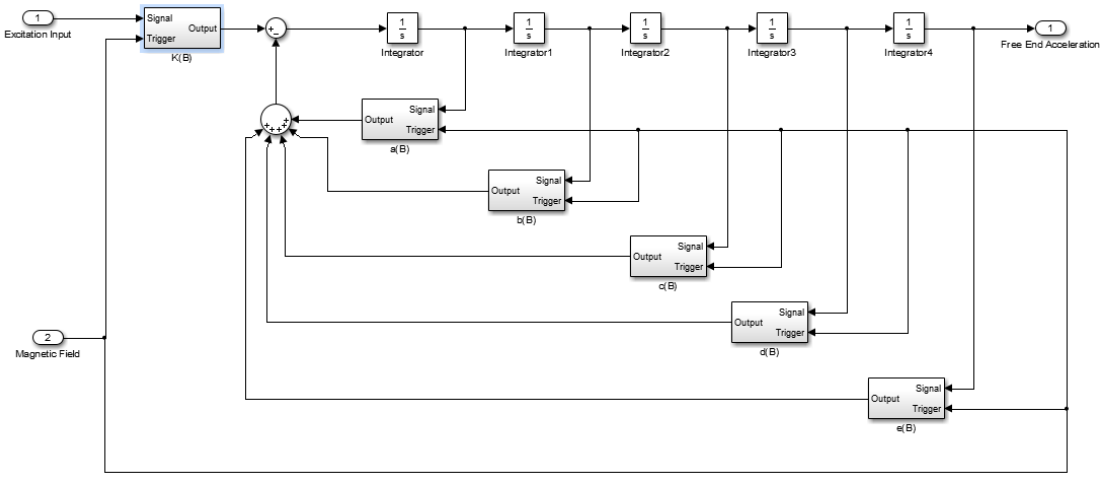

Figure 26 - MRE Sandwich Beam Model

5.8 Control

5.8.1 Procedure

The obtained gains are then used to write the LabVIEW VI to control the electromagnet - MRE Beam system.

5.8.2 LabVIEW VI

The Zoom FFT is used to get better frequency resolution of the accelerometer data. This frequency is used to simulate the model outputs for the on and off states (0mT and 285mT) of the system using the models obtained by system identification. The VI simulates and obtains the amplitude at the end of the subsequent time step. The amplitudes are compared to decide the state which provides higher amplitude reduction. Once the state to which the system is to be switched is decided. The VI changes the global state variable, which triggers the electromagnet while loop to change the state of the electromagnet (off to on, or on to off).

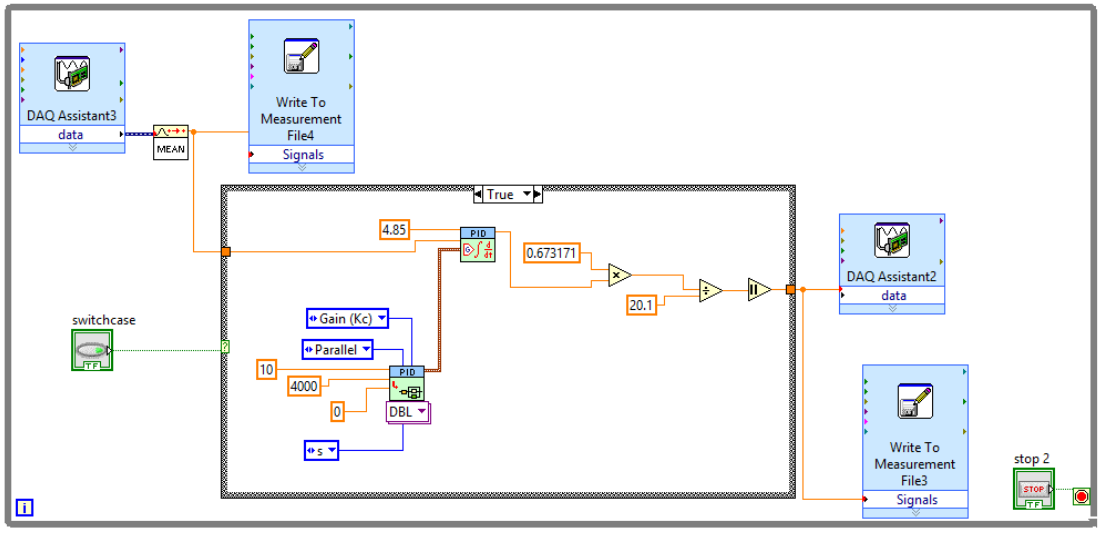

Figure 27 - Electromagnet Control Loop

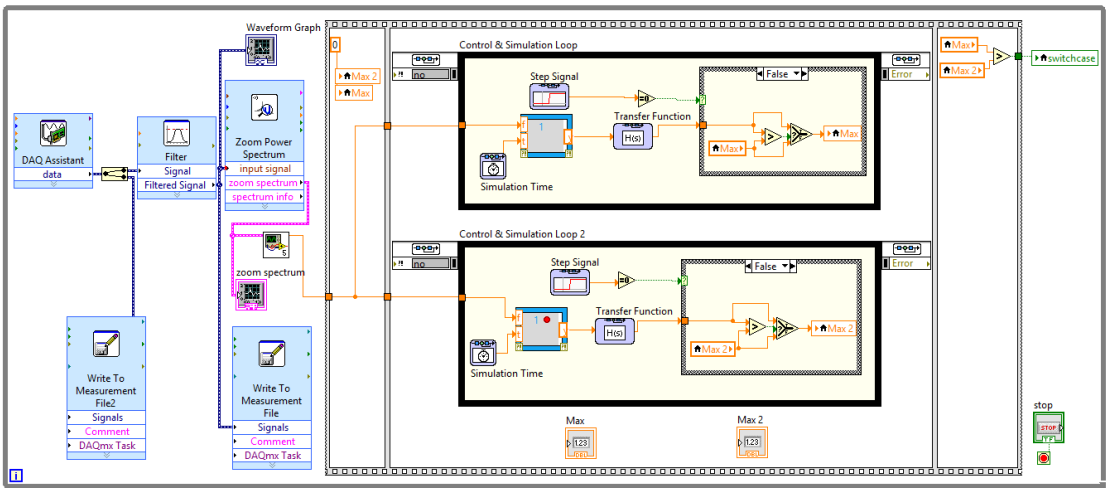

Figure 28 - On-Off Controller for MRE Sandwich Beam

Chapter 6: Results and Discussions

6.1 Free Vibration Experiment

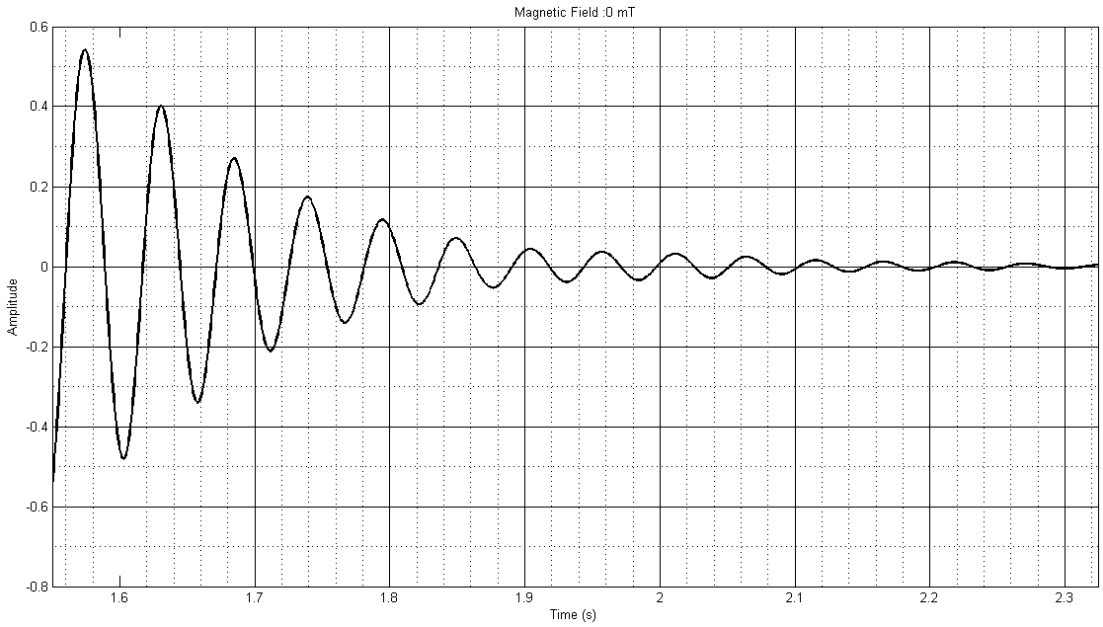

Figure 29 - Free vibration response for no magnetic field

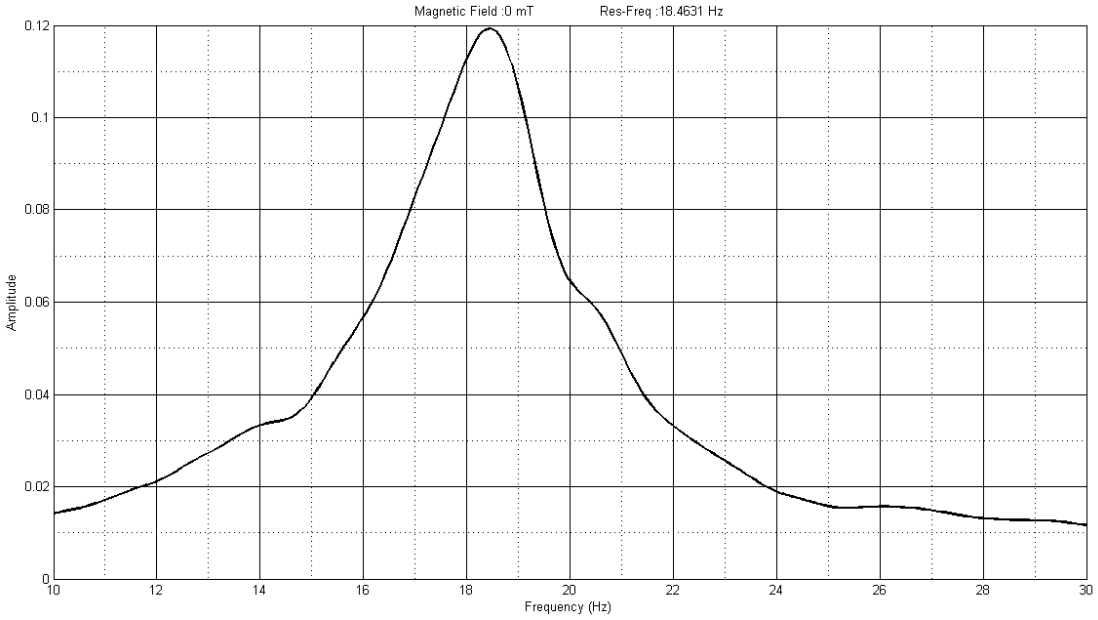

Figure 30 - FFT of time domain data for no magnetic field

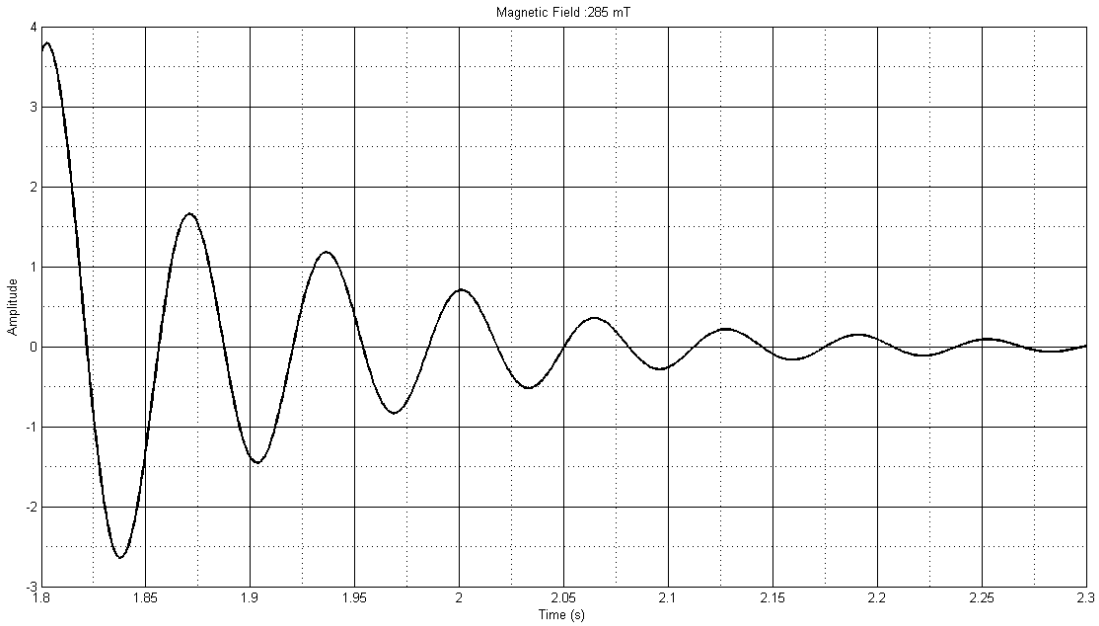

Figure 31 - Free vibration response for maximum magnetic field (285mT)

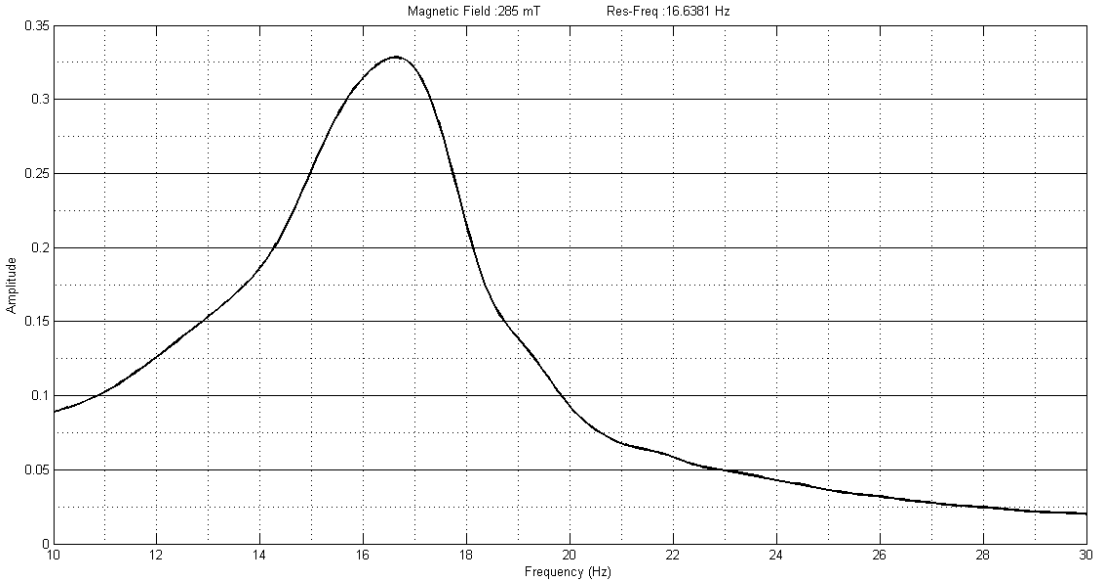

Figure 32 - FFT of time domain data for maximum magnetic field (285mT)

The natural frequency of the system under no magnetic field was found to be 18.6 Hz (Average of 15 trials). Likewise the natural frequency of the system under 285mT was found to be 16.4Hz.As observed in the literature review, the natural frequency of the beam shows a leftward shift as the magnetic field intensity increases. Thus, our experimental results are in agreement with the literature.

6.2 Impact Hammer Test

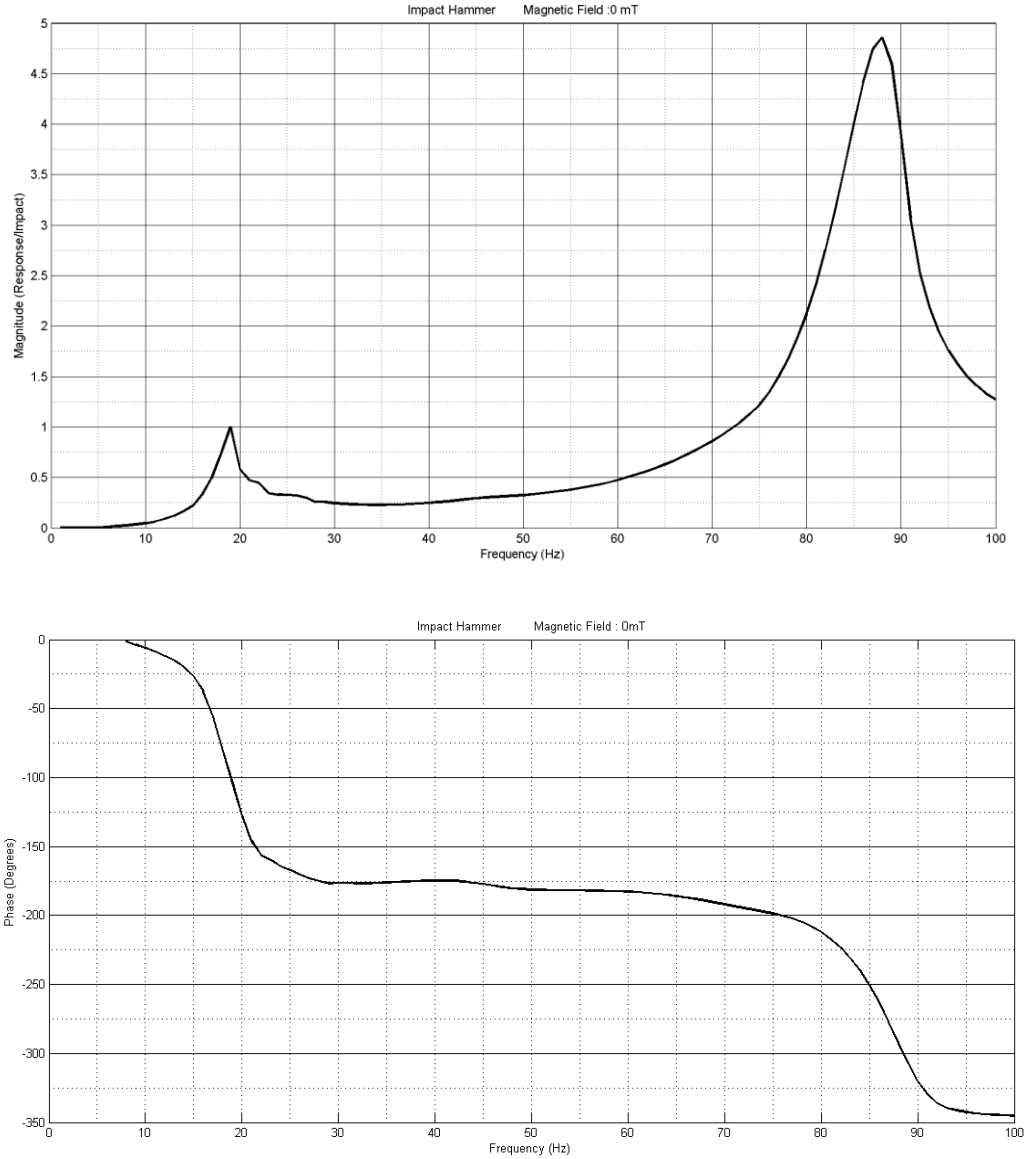

Figure 33 - Impact Hammer Test Results

a) Frequency Response b) Phase vs. Frequency c) Coherence vs. Frequency

The impact hammer test was used to identify the higher natural frequencies of the beam. The first two natural frequencies observed for zero magnetic field conditions were 18Hz and 88Hz. Coherence of 1 was observed in the range displayed.

6.3 Forced Vibration Experiment

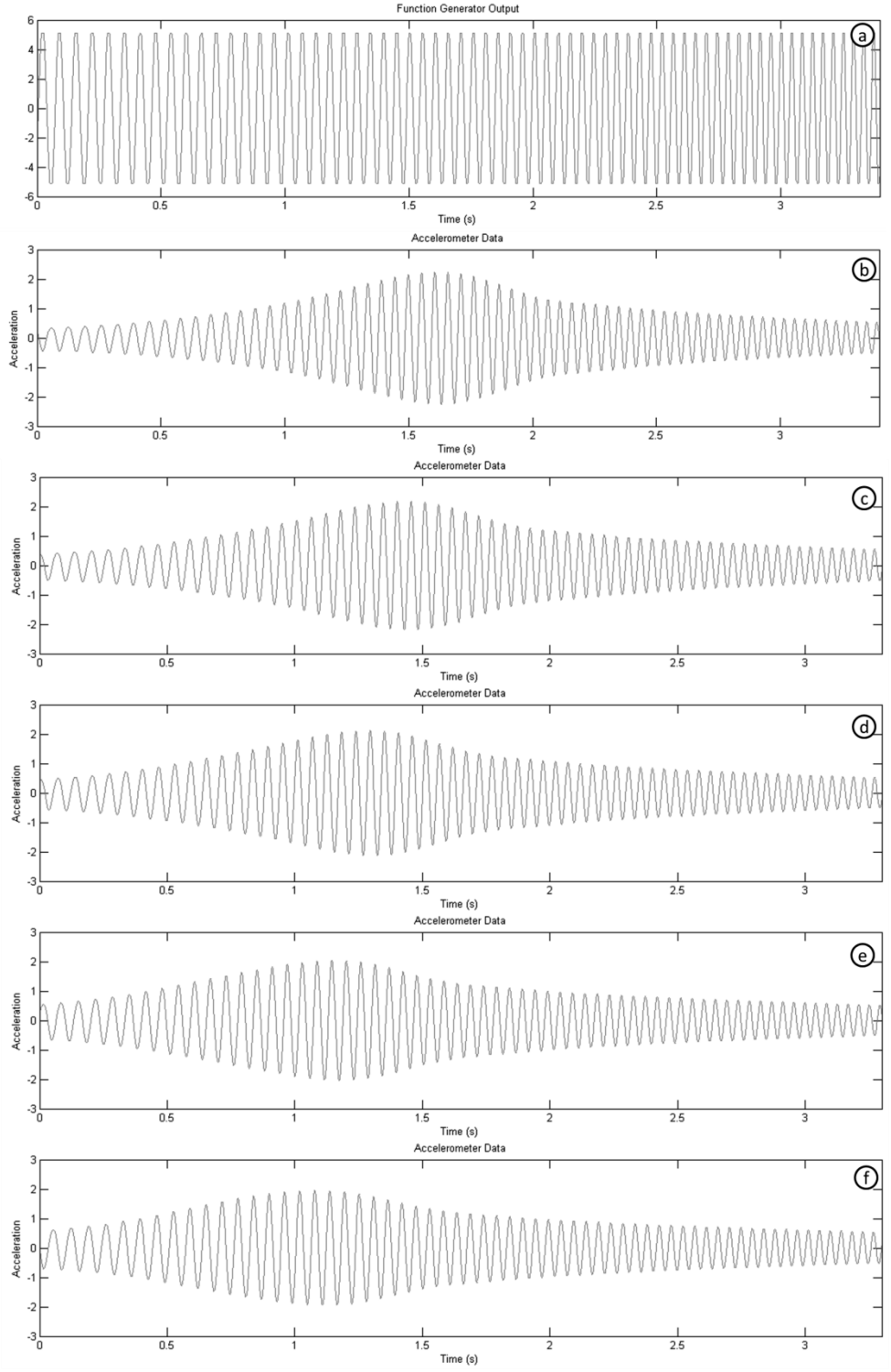

System Inputs : a) Function Generator Output
Accelerometer Outputs for Magnetic Field Conditions : b) 0mT c) 150mT d) 200mT e) 250mT f) 285mT

Figure 34 - Forced Vibration Response

The forced vibration experiment was performed with the main intention of identifying the transfer function model of the system. Figure 6.6 shows the vibration response of the system to sine sweeps from 10-25 Hz. It can be observed from Figure 34 that as the magnetic field increases the peak occurs much earlier. This is in agreement with the free vibration tests, which also showed a leftward shift in natural frequency with increase in magnetic field.

6.4 Response Time of MRE Beam to change in magnetic field

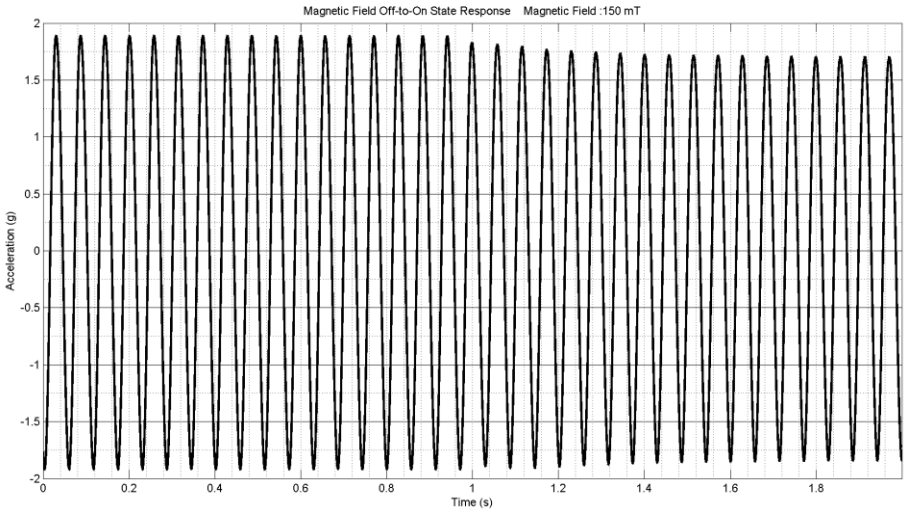

Figure 35 - Beam response to magnetic field change from off-to-on state (150mT)

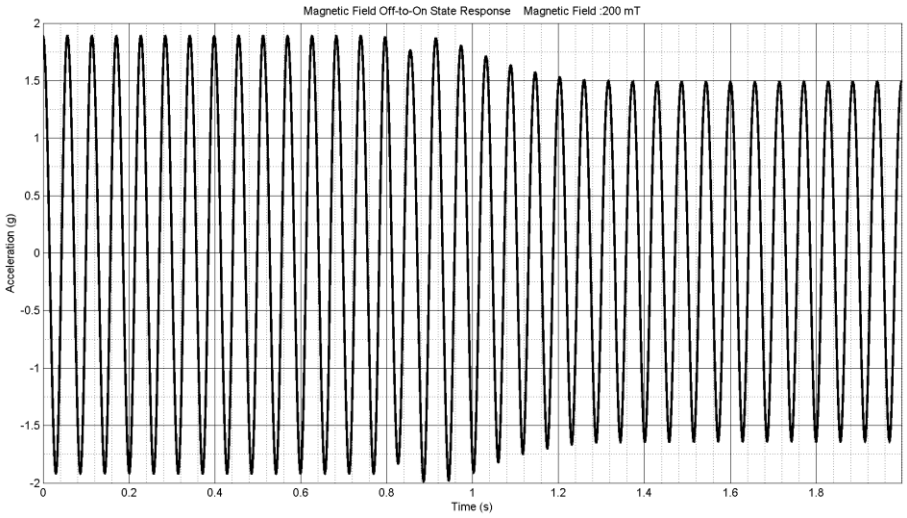

Figure 36 - Beam response to magnetic field change from off-to-on state (200mT)

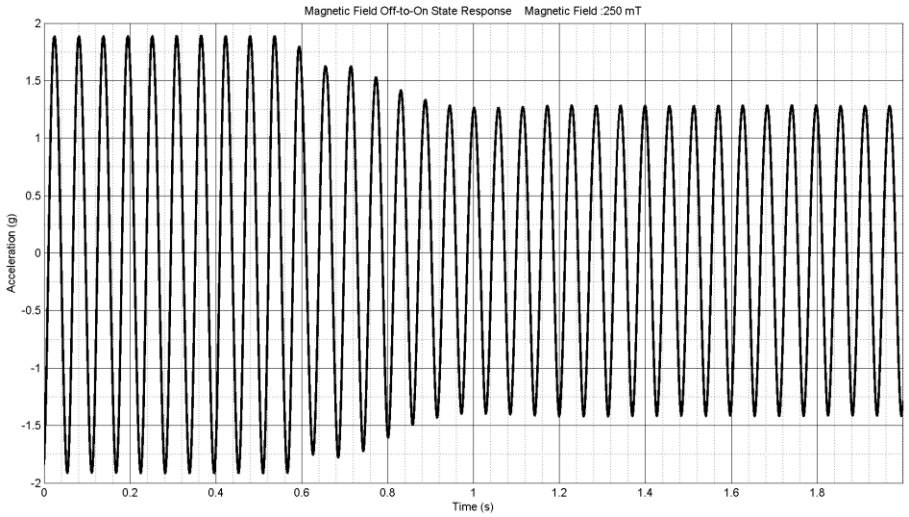

Figure 37 - Beam response to magnetic field change from off-to-on state (250mT)

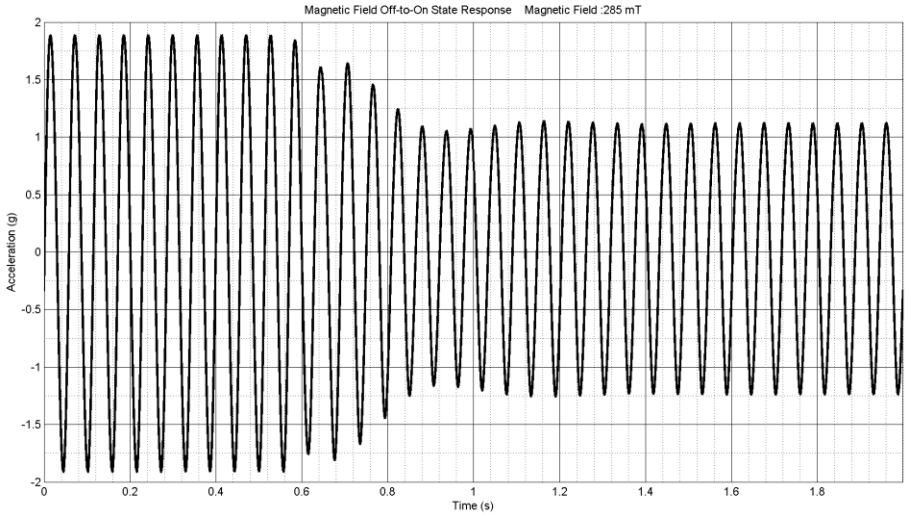

Figure 38 - Beam response to magnetic field change from off-to-on state (285mT)

The experimentally obtained data is plotted using MATLAB. The plots are used to find the response time of the MRE Beam to triggering between on and off states. The time taken for the beam to attain steady vibration amplitude after triggering is found out by tracking the peaks of each cycle of vibration.

Table 4 summarizes the data for the four field conditions and the trials taken for each case. It can be observed that the response time decreases with increasing

magnetic field. Also, it can be observed that the percentage of amplitude reduction increases with increasing magnetic field. Another observation that can be made is that the amplitude reduction for 150mT condition is very small (6.43%) when compared to the reduction achieved at 285mT (37.51%). The amplitude reduction for the lower magnetic fields 50mT, 100mT is lesser than 5% hence they have not been shown.

Magnetic Field (mT)	Trial	Off State Amplitude	On State Amplitude	Amplitude Reduction	Average	Trigger Time (s)	End Time (s)	Settling Time (s)	Average (s)
150	1	1.906	1.773	6.98%	6.43%	0.971	1.600	0.629	0.629
	2	1.905	1.789	6.06%		0.944	1.574	0.630	
	3	1.907	1.788	6.24%		0.725	1.354	0.629	
200	1	1.905	1.581	16.99%	17.24%	0.731	1.193	0.462	0.453
	2	1.906	1.581	17.05%		0.756	1.188	0.432	
	3	1.908	1.570	17.69%		0.797	1.260	0.463	
250	1	1.904	1.354	28.91%	28.92%	0.566	0.973	0.407	0.406
	2	1.898	1.353	28.72%		0.565	0.970	0.405	
	3	1.903	1.349	29.14%		0.577	0.982	0.405	
285	1	1.902	1.174	38.29%	37.51%	0.604	0.900	0.295	0.294
	2	1.903	1.202	36.86%		0.918	1.212	0.294	
	3	1.901	1.191	37.38%		0.557	0.849	0.292	

Table 4 - Consolidated data of response time of beam

6.5 Determining the Resistance and Inductance of the Electromagnet

The resistance of the electromagnet was found to be 3.8Ω. At 108Hz, the output voltage amplitude was observed to be half the input voltage.

At this point,

$$10 = \sqrt{3.8^2 + (2\pi \times 108 \times L)^2}$$

Simplifying the equation and solving for L we get,

$$L = 13.6mH$$

6.6 System Identification

The first step was for simulation was to iterate allthe model pole zero combinations, Figure 39 shows the GUI display that was obtained by performing the system model identification.

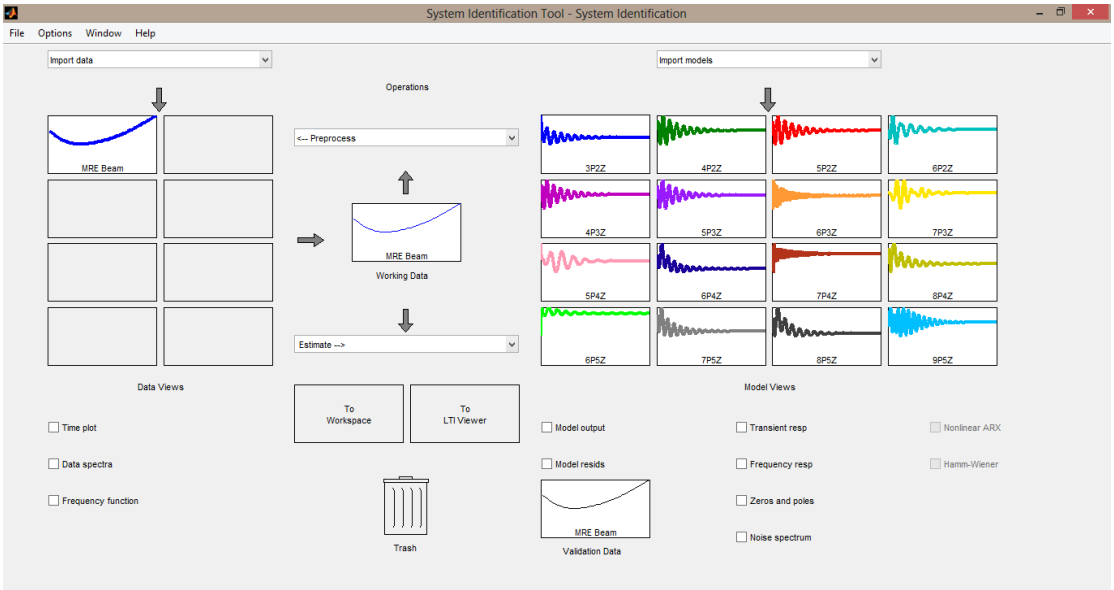

Figure 39 - MATLAB GUI after Model Iterations

The time domain data was used to compute the model output, Figure 40 shows all the model outputs along with the percentage fit of the computed model to the experimental output. It was observed that 5 Poles, 2 Zeroes model was the best fitting model to all the experimental data obtained.

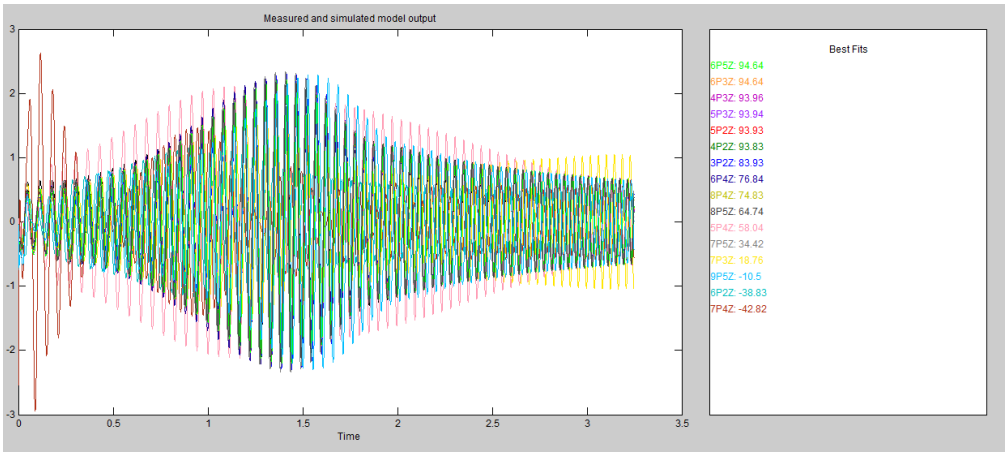

Figure 40 - Model plots with percentage fits

The Process was now iterated with all the trials for all fields, to get the poles and zeroes more precisely. Figure 41 shows the model output and fit for 0mT Field. The model fit the experimental data with 97% accuracy in relation to experimental output.

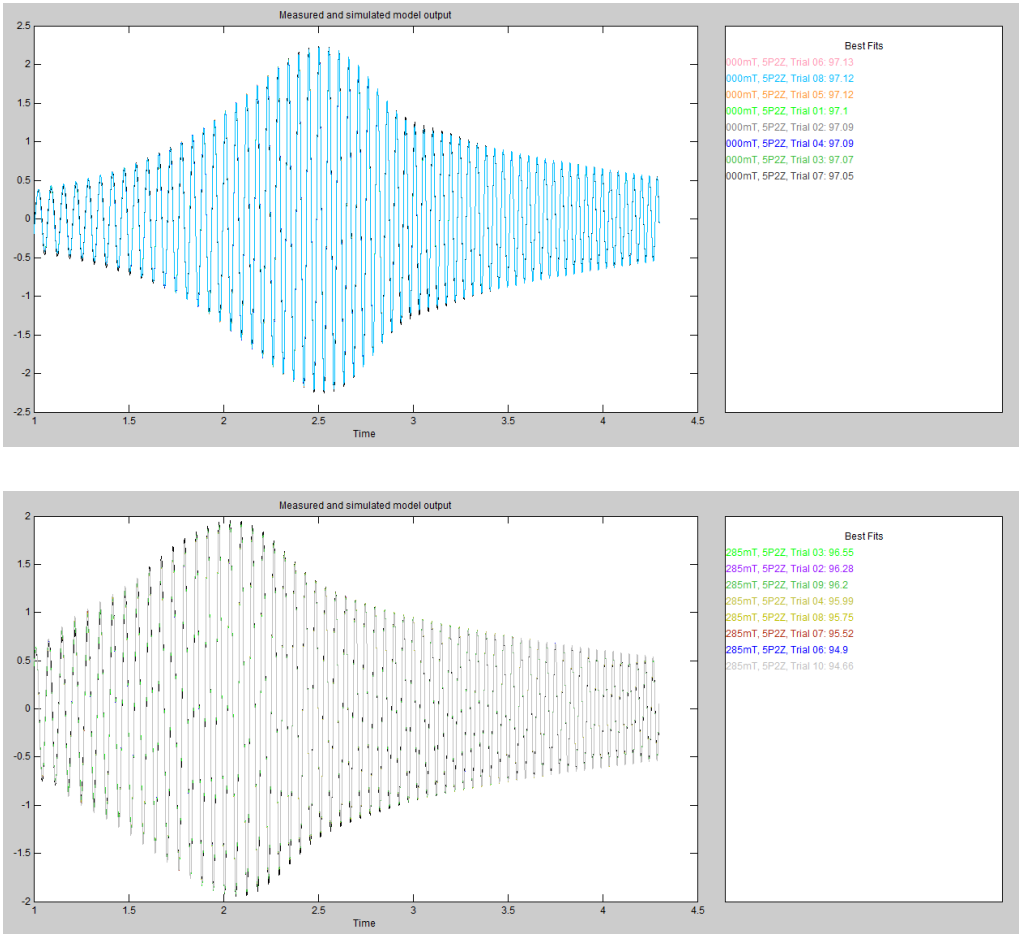

Figure 41 - Model Plots for 8 Trials at 0mT (Top) and 285mT (Bottom)

Figure 41 shows the model output and fit for 285mT Field. The model fit the experimental data with about 95% accuracy in relation to experimental output.

The frequency response of all the models was computed and is shown in Figure 42. It can be seen that the peaks shift leftward as magnetic field increases. Also the peaks were observed at 18.5Hz and 16.4 Hz which are in accordance with the free vibration results. Another observation from Figure 42 is that the peak amplitude is decreasing as magnetic field increases. This reduction in resonant frequency

amplitude can be attributed to increasing damping ration (zeta) as magnetic field increases.

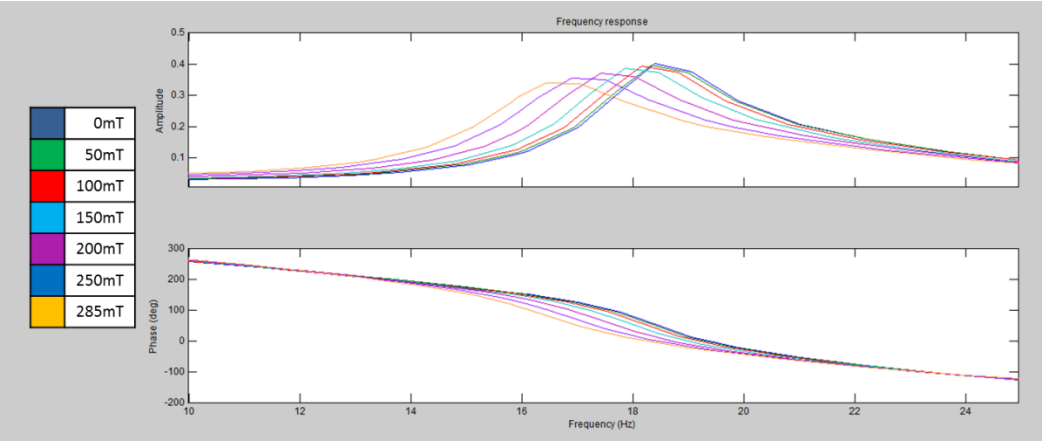

Figure 42 - Frequency Response for different magnetic fields

The model poles and zeros were plotted to observe the trend in which the open loop poles and zeroes of the system move as magnetic field increases. This is shown in Figure 43.

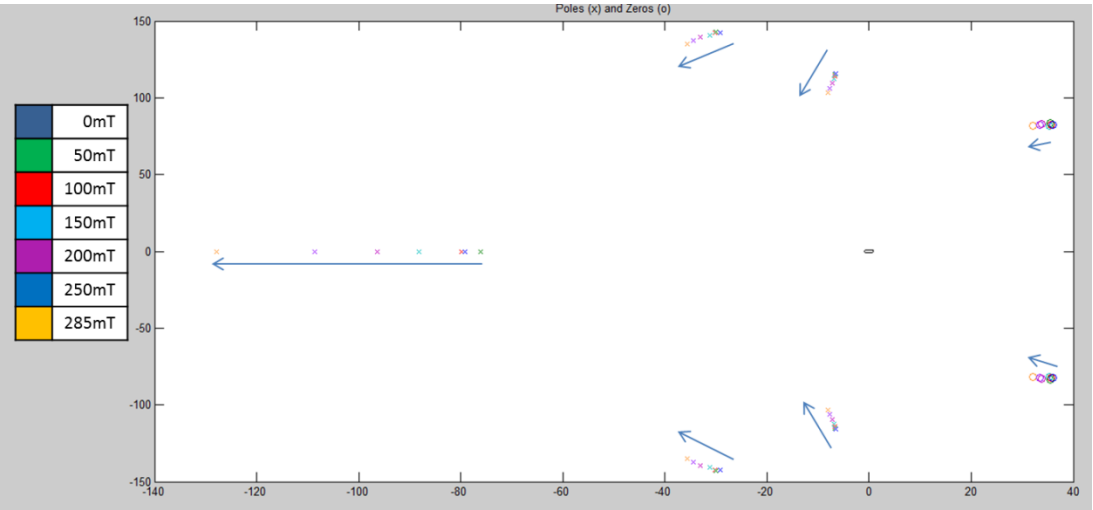

Figure 43 - Poles and Zeroes for different magnetic fields

The corresponding transfer function is as follows:

$$Transfer\ Function = \frac{a_2 s^2 + a_1 s + a_0}{b_5 s^5 + b_4 s^4 + b_3 s^3 + b_2 s^2 + b_1 s + b_0}$$

Where,

B	a_2	a_1	a_0
0mT	8.924e04	-6.432e06	7.188e08
285mT	1.517e05	-9.652e06	1.225e09

B	b_5	b_4	b_3	b_2	b_1	b_0
0mT	1	150.8	4.105e04	3.866e06	3.689e08	2.254e10
285mT	1	209.3	4.239e04	4.881e06	3.449e08	2.516e10

Table 5 - Model Constants for Off and On State

6.7 Simulation

The SIMULINK model was used to simulate the sine sweep response to check the accuracy of the model. The model simulated the response with accuracy of 96%. The graphs of the input signal, simulated output and actual output are shown in Figure 44.

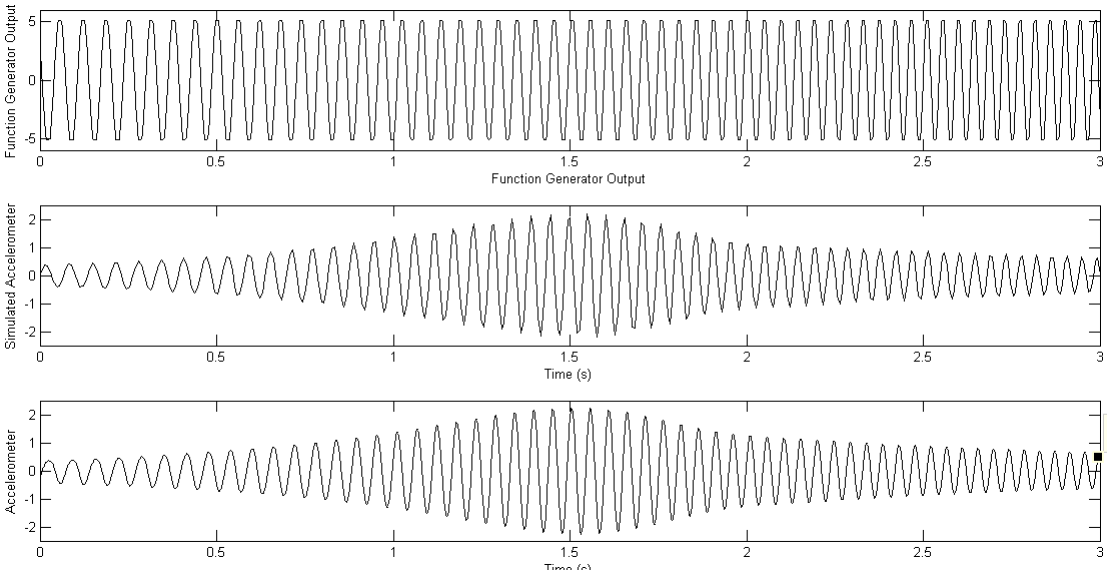

Figure 44 - Sine Sweep Simulations in SIMULINK

The Off-to-On state was simulated in SIMULINK to check the response of the system when voltage steps are applied to the electromagnet coils. The final steady state amplitudes were within 10% error. Figure 45 shows the actual and simulated response of the system when subjected to state change from off to on.

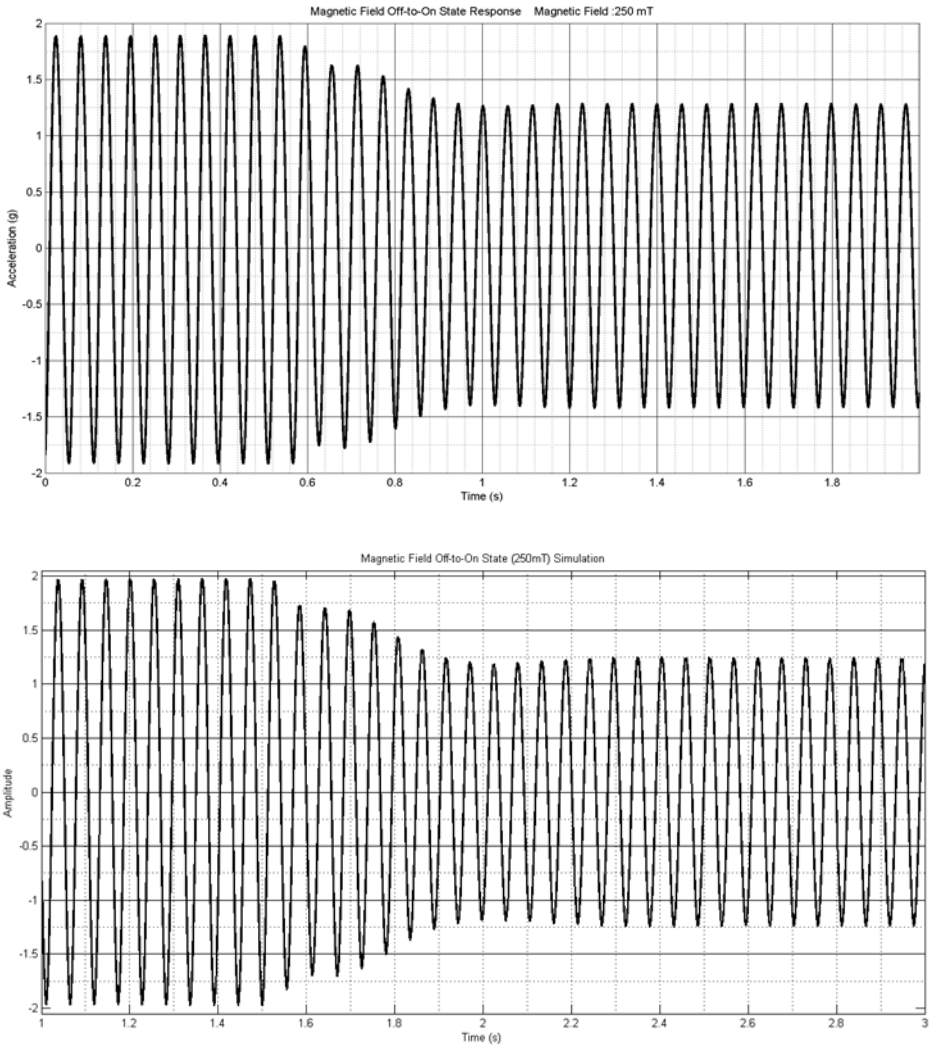

Figure 45 - Off to On State Simulation in SIMULINK

6.8 On-Off Controller

The On-Off controller results are shown in Figure 46 and Figure 47. The algorithm triggers the state from On-to-Off or Off-to-On depending on the case which

would produce lower amplitudes by using the models estimated from system identification. 50% reduction in amplitude was obtained at the resonance frequency.

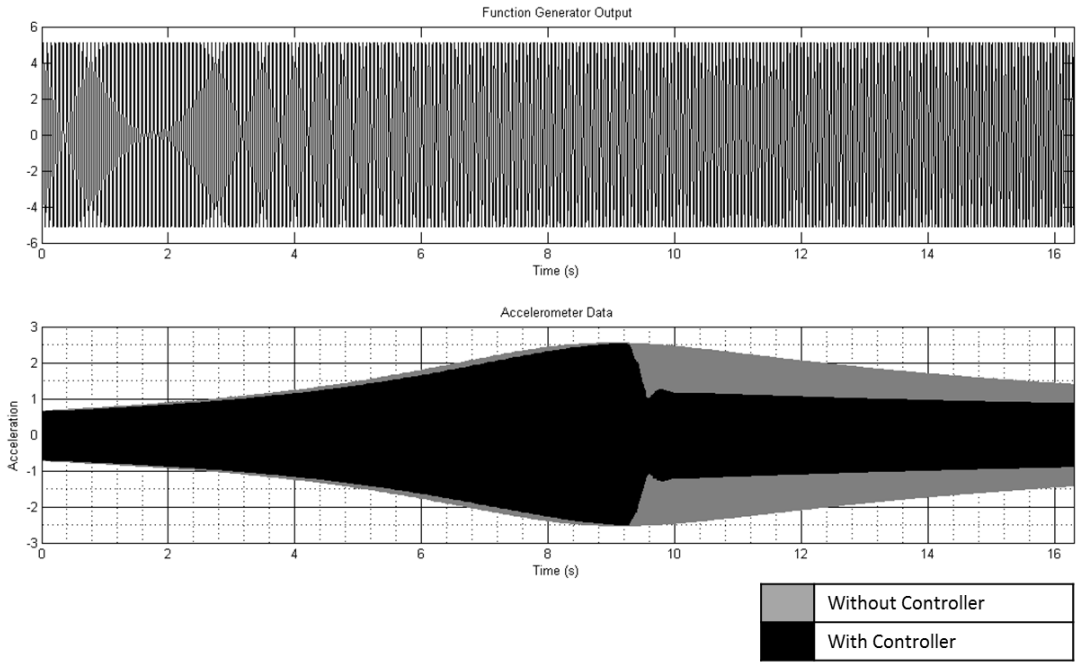

Figure 46 - Accelerometer output with and without controller

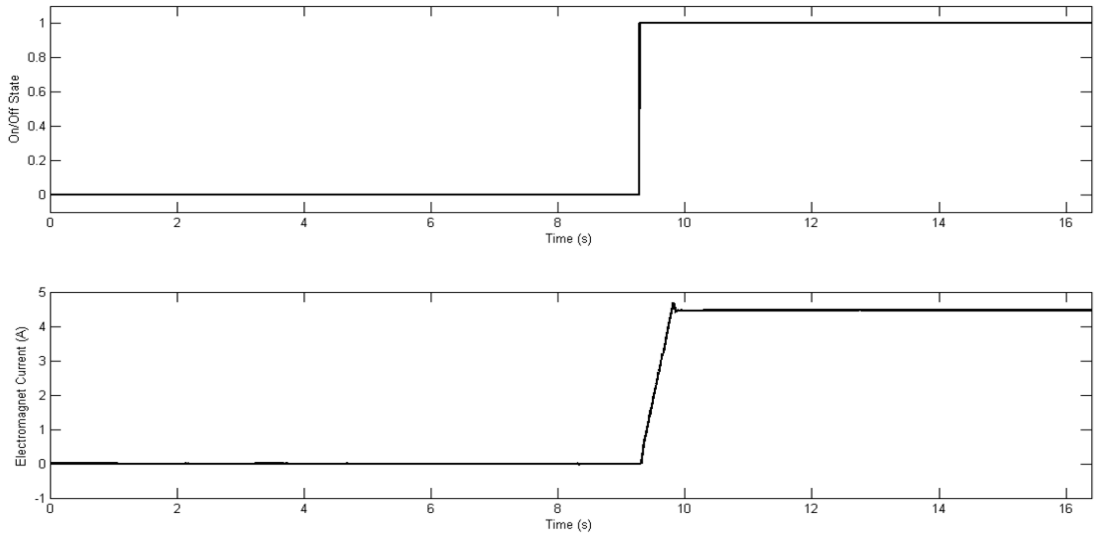

Figure 47 - Control Algorithm Trigger Point and Electromagnet Current vs. Time

Chapter 7: Conclusions and Future Scope

In this project the system was modelled using System identification tool box in MATLAB and model validation was done in SIMULINK. On-Off controller was used to attenuate the vibration of the beam based on both, the amplitude of vibration and the natural frequency of the beam. A comparison of the displacement and acceleration of the beam with the controller and without the controller proved that the controller effectively reduces the system response. This control logic can significantly reduce the displacement and acceleration. A reduction of 50% in the amplitude of acceleration was achieved using the On-Off controller. Thus, in comparison to the passive control system, the semi-active controller is more appropriate approach for vibration control.

Future work:

In the present work, the magnetic field is applied non-homogenously to only one region of the beam. The future work may be divided as follows

1) The position of the application of magnetic field can be varied along the length of the beam and the effect can be studied.
2) Implementing and finding alternate control logics for vibration control. By comparing the vibration response of displacement and acceleration for different control algorithms, reasonable control logic with satisfactory control can be selected and studied.
3) Phenomenological Modelling of the MRE can be done using rheometer and this can be used to directly incorporate the magnetic field effect on the system model.

REFERENCES

1) Hu, G., Guo, M., Li, W., Du, H. & Alici, G. (2011). Experimental investigation of the vibration characteristics of a magnetorheological elastomer sandwich beam under non-homogeneous small magnetic fields. Smart Materials and Structures, 20 (12), 1-7.
2) Li, W. H., Zhang, X. Z. & Du, H. (2013). Magnetorheological elastomers and their applications. In P. M. Visakh, S. Thomas, A. K. Chandra & A. P. Mathew (Eds.), Advances in Elastomers I: Blends and Interpenetrating Networks (pp. 357-374). Berlin, Germany:Springer.
3) Yang Zhou, 2009. MR Elastomers for Structural Control. Masters thesis, Faculty of Engineering, University of Wollongong.
4) Liao G J, Gong X L, Xuan S H, Kang C J and Zong L H (2011). Development of a real-time tunable stiffness and damping vibration isolator based on magnetorheological elastomer. Journal of Intelligent Material Systems and Structures 23(1) 25–33.
5) Liao G J, Gong X L, Kang C J and Xuan S H (2011).The design of an active–adaptive tuned vibration absorber based on magnetorheological elastomer and its vibration attenuation performance.Smart Mater. Struct., 20(10), 075015.
6) Kaleta Jerzy, Michał Krolewicz and Daniel Lewandowski (2011).Magneto mechanical properties of anisotropic and isotropic magnetorheological composites with thermoplastic elastomer matrices.Smart Mater. Struct.2 (12)85006.
7) Dong Xiao-min, Yu Miao, Liao Chang-rong, Chen Wei-min (2009). A new variable stiffness absorber based on magneto-rheological elastomer. Transaction of nonferrous metal society of china, 19(6), 611-615.
8) Li Yancheng, Jianchun Li , Weihua Li and Haiping Du (2014).A state-of-the-art review on Magnetorheological elastomer devices.” Smart Mater. Struct. 23(24), 123001.
9) System Identification Tool Box Manual, MATLAB.